The effect of surface steps and oxides on the catalytic activity on model Pd and Rh catalysts

Zhang, Chu

2018

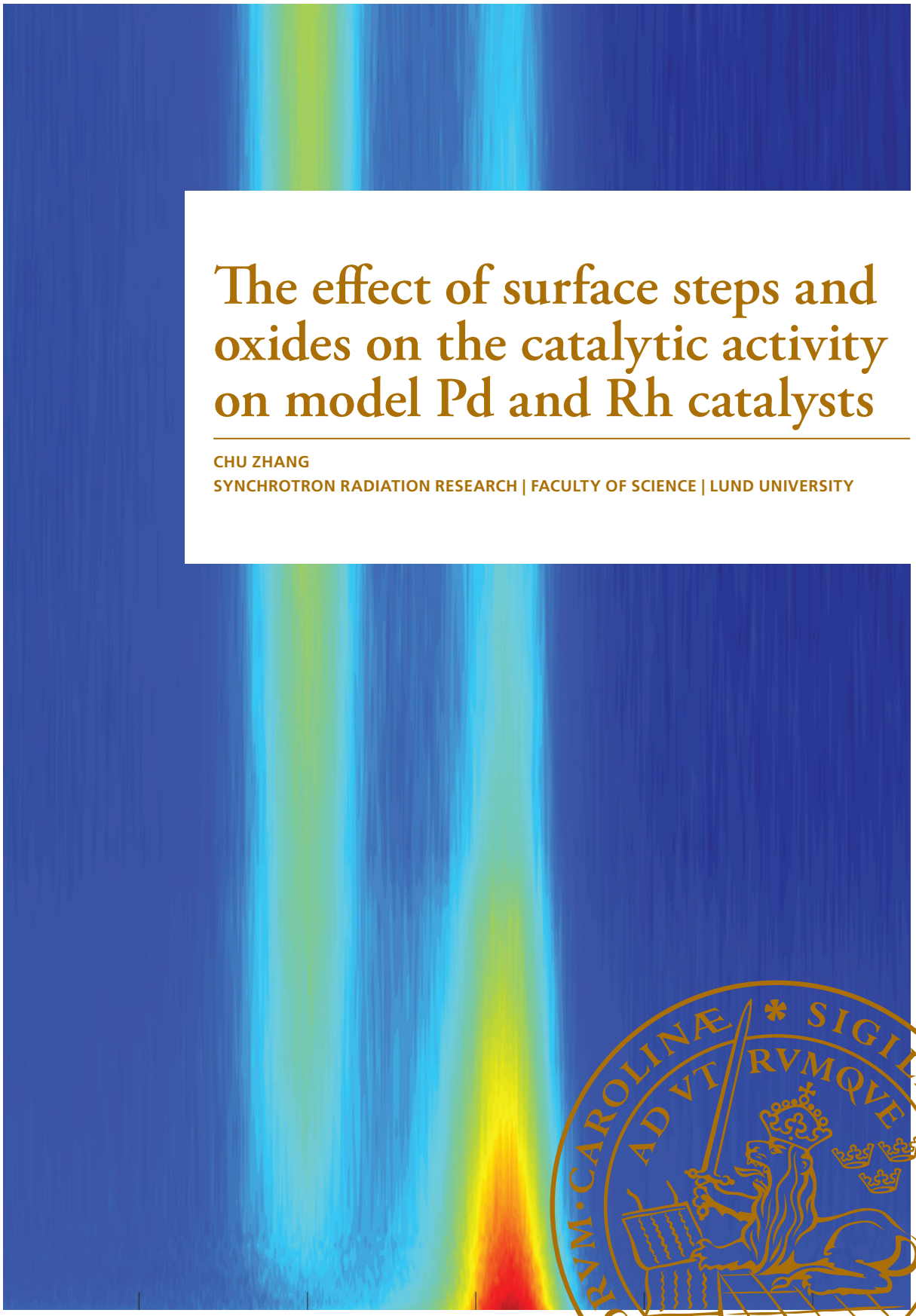

The effect of surface steps and oxides on the catalytic activity on model Pd and Rh catalysts

CHU ZHANG
SYNCHROTRON RADIATION RESEARCH | FACULTY OF SCIENCE | LUND UNIVERSITY

Printed by Media-Tryck, Lund 2018 NORDIC SWAN ECOLABEL 3041 0903

Lund University
Faculty of Science
Department of Physics
Division of Synchrotron Radiation Research
ISBN 978-91-7753-800-4

The effect of surface steps and oxides on the catalytic activity on model Pd and Rh catalysts

by Chu Zhang

Division of Synchrotron Radiation Research

LUND
UNIVERSITY

DOCTORAL THESIS

by due permission of the Faculty of Science, Lund University, Sweden.

To be defended in the Rydberg Lecture Hall at the Department of Physics, Sep 13, 2018, at 09:15

Dissertation advisors

Dr. Johan Gustafson, Prof. Edvin Lundgren

Faculty opponent

Anne Borg

Organization
LUND UNIVERSITY
Division of Synchrotron Radiation Research
Department of Physics, Box 118, S-221 00 Lund

Document name
DOCTORAL DISSERTATION

Date of disputation
2018-09-13

Sponsoring organization

Author(s)
Chu Zhang

Title and subtitle
The effect of surface steps and oxides on the catalytic activity on model Pd and Rh catalysts

Abstract
A catalyst is a substance that can speed up the rate of a chemical reaction without itself being consumed. Catalysts are crucial for chemical production industries, where about 90% of all chemicals are produced using catalysts. They are also used for exhaust gas cleaning, for instance in cars, where CO and unburned fuels are oxidized to CO_2 and NO_x is reduced to N_2. To optimize catalysts, and develop other or better catalysts in the future, we need to know how they work on the atomic level.

Industrial catalysts are complicated, consisting of active nanoparticles dispersed in a porous oxide support and working under atmospheric or higher pressures. Therefore, it is challenging to study the surface structure. The surface is crucial because it is the part of the catalyst that interacts with the surrounding gas, and hence is where the catalytic reaction occurs. To be able to study the surface in detail, researchers in the field of surface science study simplified systems, typically perfectly flat single crystals in ultra-high vacuum. This enables very detailed studies but can suffer from being too simplified. The difference in working pressures and complexity between surface science and industrial catalysis are called the pressure and material gaps.

In this thesis, I have taken one step to bridge these gaps for CO oxidation over Rh and Pd. More specifically, I have studied the effect of steps, which are always present on the nanoparticles in industrial catalysts, by studying so-called vicinal single crystal surfaces with a well ordered periodic array of steps. Furthermore, I have studied the role of oxides for the catalytic activity.

My results show that the presence of steps improves the catalytic activity. It is, however, not the steps as such that are most active, but the flat surface near the steps. Further, the activity of the oxides I have studied depends on their surface structure. If there are sites available for CO to adsorb, the oxide is active, while, for instance, the oxygen terminated Rh oxide shows low activity. These results may be used to optimize the structure and composition of catalysts to expose a perfect density of steps and/or active oxides.

Key words
Surface X-ray diffraction, X-ray photonelectron spectroscopy, Catalytic activity, Oxide, Single Crystal surface, Surface structure, vicinal surface, CO oxidation, stepped surface

Classification system and/or index terms (if any)

Supplementary bibliographical information

Language
English

ISSN and key title

ISBN
978-91-7753-800-4 (print)
978-91-7753-801-1 (pdf)

Recipient's notes

Number of pages
84

Price

Security classification

Signature 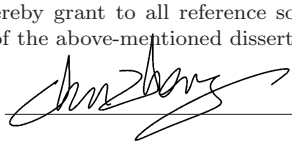

Date 2018-08-13

The effect of surface steps and oxides on the catalytic activity on model Pd and Rh catalysts

by Chu Zhang

Division of Synchrotron Radiation Research

LUND
UNIVERSITY

DOCTORAL THESIS

Cover illustration front: O 1*s* spectra of reduction of preadsorbed O from Rh(553).

Doctoral dissertation
Division of Synchrotron Radiation Research
Department of Physics
Lund University

ISBN: 978-91-7753-800-4 (print)
ISBN: 978-91-7753-801-1 (pdf)

Printed in Sweden by Media-Tryck, Lund University, Lund 2018

Dedicated to my loving parents, my husband my adorable daughter

Abstract

A catalyst is a substance that can speed up the rate of a chemical reaction without itself being consumed. Catalysts are crucial for chemical production industries, where about 90% of all chemicals are produced using catalysts. They are also used for exhaust gas cleaning, for instance in cars, where CO and unburned fuels are oxidized to CO_2 and NO_x is reduced to N_2. To optimize catalysts, and develop other or better catalysts in the future, we need to know how they work on the atomic level.

Industrial catalysts are complicated, consisting of active nanoparticles dispersed in a porous oxide support and working under atmospheric or higher pressures. Therefore, it is challenging to study the surface structure. The surface is crucial because it is the part of the catalyst that interacts with the surrounding gas, and hence is where the catalytic reaction occurs. To be able to study the surface in detail, researchers in the field of surface science study simplified systems, typically perfectly flat single crystals in ultra-high vacuum. This enables very detailed studies but can suffer from being too simplified. The difference in working pressures and complexity between surface science and industrial catalysis are called the pressure and material gaps.

In this thesis, I have taken one step to bridge these gaps for CO oxidation over Rh and Pd. More specifically, I have studied the effect of steps, which are always present on the nanoparticles in industrial catalysts, by studying so-called vicinal single crystal surfaces with a well ordered periodic array of steps. Furthermore, I have studied the role of oxides for the catalytic activity.

My results show that the presence of steps improves the catalytic activity. It is, however, not the steps as such that are most active, but the flat surface near the steps. Further, the activity of the oxides I have studied depends on their surface structure. If there are sites available for CO to adsorb, the oxide is active, while, for instance, the oxygen terminated Rh oxide shows low activity. These results may be used to optimize the structure and composition of catalysts to expose a perfect density of steps and/or active oxides.

Popular Science Summary

A catalyst is a substance that can speed up the rate of a chemical reaction without consume or change itself is commonly used for chemical production and for car exhaust gas cleaning process to remove for instance toxic gases such as CO and NO. In order to optimize the catalyst and to develop other or better catalysts in the future, we need to know how the catalyst work on the atomic level. Industrial catalysts are complex, making it difficult to study their surface structure. The surface of the catalyst is important because it interacts with the sourrounding gas, namely, the surface structure directly affects the catalytic activity. Instead of using the complex material system used in industry, we use the so-called surface science approach, which means we simplify the material to single crystal and the reaction condition to ultra high vacuum conditions, in contrast to the industry working with complex nanoparticle at atmospheric ambient or higher pressures. Because of the complexity of industrial catalysts and the harsh operating environment, we can not study the surface of the catalytic material directly, on the another hand, a too simple model system is also a problem. Therefore, we want to use conditions more similar to industrial conditions but still maintaining control over the catalyst surface and the gas environment, decreasing the so-called pressure and material gaps.

In this thesis, I have tried to bridge these gaps. The catalytically active nanoparticles in an industrial catalyst have defects such as steps, kinks and corners. To investigate the influence of such defects on the catalytic activity, I investigated flat surfaces as well as surfaces with a high density of defects, so-called low index and vicinal surfaces, respectively. Further, under more realistic conditions, oxides are believed to play an important role in an industrial catalyst, and therefore the effect of the oxide on the catalytic activity is also studied. In this thesis, I studied the vicinal Rh(553) and Pd(553) surfaces. I found that when exposing Rh(553) to the catalytic reaction condition, the surface will rearrange into different facets, meaning the distance between the step changes. To investigate how the stepped surface influence the activity, the (331) was studied in more detail. The catalytic activity for CO oxidation varies depending on the surface structure and step density. Pd(553) also rearrange during reaction condition, but form different facets as compared to Rh(553). Concerning the catalytic activity on oxide surfaces, the Rh oxides are inactive, the Rh is active in the metallic phase. The activity of Pd oxides depends on their thickness and their resulting change in surface structure. The result presented in this thesis also show that the presence of steps is important for the catalytic activity, however, if the steps are too close to each other, the catalyst will be less active, the optimized step density is good for maximizing activity.

Populärvetenskaplig sammanfattning

En katalysator är en substans som kan snabba på en kemisk reaktion utan att själv förbrukas. Katalysatorer används vanligen i kemisk produktion och i bilars förbränningsmotorer (för att ta bort tex CO och NO). För att optimera katalysatorn och utveckla andra och bättre katalysatorer i framtiden så behöver vi veta hur katalysatorn fungerar på atomär nivå. Katalysatorer i industrin är komplexa vilket gör det svårt att studera deras ytstrukturer. Ytan på katalysatorn är viktig då den interagerar med den omgivande gasen, ytstrukturen har en direkt påverkan på processen. Istället för att använda de komplexa materialsystem som används inom industrin så använder vi en ytvetenskaplig metod vilket betyder att vi förenklar materialet till enkristallina material och låter reaktionerna ske i ultrahögt vakuum. Detta i kontrast till industrins komplexa nanopartiklar vid atmosfärstryck eller högre. På grund av de komplexa systemen och tuffa reaktionsmiljöerna i industrin så kan vi inte direkt studera dessa system, men inte heller bör vi förenkla systemet för mycket. Vi vill så gott vi kan efterlikna de villkor som finns i industrin utan att för den sakens skull förlora kontroll över ytan eller dess omgivning, på så sätt vill vi övervinna det vi ofta kallar för "tryck-gapet" och "material-gapet".

I den här avhandlingen har jag försökt att överbrygga dessa gap. Den katalytiskt aktiva nanopartikeln i en industriell katalysator har ytdefekter såsom atomära steg och hörn. För att studera inflytandet av sådana defekter på den katalytiska processen så jämför jag katalysatorer med helt platta ytor med katalysatorer med ytor som innehåller många defekter, så kallade låg-index och vicinala ytor. Dessutom, i mer realistiska miljöer så tros oxider spela en viktig roll för den industriella katalysatorn, därför studerar vi även oxiders effekt på den katalytiska aktiviteten. I den här avhandlingen studerar jag de vicinala Rh(553)- och Pd(553)-ytorna. Jag upptäckte att då man exponerar Rh(553) för den katalytiska reaktionen så omfördelas atomerna på ytan till olika facetter vilket betyder att steglängden förändras. För att undersöka hur den nya ytan påverkar den katalytiska aktiviteten så studerades (331) i mer detalj. Den katalytiska aktiviteten för CO-oxidation varierar beroende på ytstrukturen och stegdensiteten. Pd(553) omfördelas också under reaktionen men bildar andra facetter än Rh(553). Angående den katalytiska aktiviteten på ytor med oxider så Rh är aktivt i dess metalliska fas, Rh-oxiderna inaktiva och aktiviteten hos Pd-oxiderna varierar med dess tjocklek och deras slutliga ytstruktur. Resultaten som presenteras i den här avhandlingen visar också att förekomsten av atomära steg spelar en viktig roll för den katalytiska aktiviteten. Om stegen är för nära varandra så är inte katalysatorn aktiv. Att finna den optimala stegdensiteten är bra för att maximera aktiviteten.

Preface

This thesis is based on the following publications, referred to by their Roman numerals:

I – Faceting of Rhodium(553) in Realistic Reaction Mixtures of Carbon Monoxide and Oxygen

C. Zhang, E. Lundgren, P.-A. Carlsson, O.Balmes, A. Hellman, L. R. Merte, M. Shipilin, W. Onderwaater, J. Gustafson
J. Phys. Chem. C 119, 11646-11652, **2015**. DOI: 10.1021/acs.jpcc.5b01841

My contribution: I was main responsible for the experiments, performed the data analysis, and was main responsible for writing the paper.

II – Steps and Catalytic Reactions: CO Oxidation with Preadsorbed Oxygen on Rh(553)

C. Zhang, B.C. Wang, M. Shipilin, A. Schaefer, L. R. Merte, S. Blomberg, X.T. Wang, P.-A. Carlsson, E. Lundgren, A. Hellman, J. Gustafson
Submitted

My contribution: I was main responsible for the experiments, performed the data analysis, and was main responsible for writing the paper.

III – A Study of Reduction of Oxygen Structures on a Faceted Rh(553) Surface by CO

C. Zhang, M. Shipilin, A. Schaefer, L. R. Merte, S. Blomberg, X.T. Wang, P.-A. Carlsson, E. Lundgren, J. Gustafson
In manuscript

My contribution: I was main responsible for the experiments, performed the data analysis, and was main responsible for writing the paper.

IV – Step Dynamics and Oxide Formation During CO Oxidation over a Vicinal Pd Surface

M. Shipilin, J. Gustafson, **C. Zhang**, L. R. Merte, E. Lundgren
Phys. Chem. Chem. Phys. 18, 20312-20320, **2016**. DOI: 10.1039/c5cp07488f

My contribution: I participated in the experiments and contributed to the discussion of the results and paper writing.

V – **The Role of Oxides in Catalytic CO Oxidation over Rhodium and Palldium**

J. Gustafson, O.Balmes, **C. Zhang**, M. Shipilin, A. Schaefer, B. Hugman, L. R. Merte, N.M. Martin, P.-A. Carlsson, M. Jankowski, E.J. Crumlin, E. Lundgren
ACS Catal, 8, 4438-4445, **2018**. DOI: 10.1021/acscatal.8b00498

My contribution: I participated in the experiments and contributed to the discussion of the results and paper writing.

VI – **High-Energy Surface X-ray Diffraction for Fast Surface Structure Determination**

J. Gustafson, M. Shipilin, **C. Zhang**, A. Stierle, U. Hejral, U. Ruett, O. Gutowski, P.-A. Carlsson, M. Skoglundh, E. Lundgren
Science 343(6172), 758-761, **2014**. DOI: 10.1126/science.1246834

My contribution: I participated in the experiments and contributed to the discussion of the results and paper writing.

Publications related but not included in the present dissertation:

An In Situ Sample Environment Reaction Cell for Spatially Resolved X-Ray Absorption Spectroscopy Studies of Powders and Small Structured Reactors

C. Zhang, J. Gustafson, L. R. Merte, J. Evertsson, K. Noren, S. Carlson, H. Svensson, P.-A. Carlsson
Rev. Sci. Instruments. 86, 033112, **2015**. DOI: 10.1063/1.4915321

Quantitative Surface Structure Determination Using In Situ High-Energy SXRD: Surface Oxide Formation on Pd(100) During Catalytic CO Oxidation

M. Shipilin, U. Hejral, E. Lundgren, L. R. Merte, **C. Zhang**, A. Stierle, U. Ruett, O. Gutowski, M. Skoglundh, P.-A. Carlsson, J. Gustafson
Surf. Sci. 630, 229-235, **2014**. DOI: 10.1016/j.susc.2014.08.021

High-Energy X-Ray Diffraction from Surfaces and Nanoparticles

U. Hejral, P. Müller, M. Shipilin, J. Gustafson, D. Franz, R. Shayduk, U. Rütt, **C. Zhang**, L. R. Merte, E. Lundgren, V. Vonk, A. Stierle
Phys. Rev. B. 96, 195433, **2017**. DOI: 10.1103/PhysRevB.96.195433

The Influence of Incommensurability on the Long Range Periodicity of the Pd(100)-($\sqrt{5} \times \sqrt{5}$)R27°-PdO(101)

M. Shipilin, A. Stierle, L. R. Merte, J. Gustafson, U. Hejral, N. M. Martin, **C. Zhang**, D. Franz, V. Kilic, E. Lundgren
Surf. Sci. 660, 1-8, **2017**. DOI: 10.1016/j.susc.2017.01.009

Fe Oxides on Ag Surfaces: Structure and Reactivity

M. Shipilin, E. Lundgren, J. Gustafson, **C. Zhang**, F. Bertram, C. Nicklin, C. J. Heard, H. Grönbeck, F. Zhang, J. Choi, V. Mehar, J. F. Weaver, L. R. Merte
Top Catal. 60, 492-502, **2017**. DOI: 10.1007/s11244-016-0714-8

Growth of Ultrathin Iron Oxide Films on Ag(100)

L. R. Merte, M. Shipilin, S. Ataran, S. Blomberg, **C. Zhang**, A. Mikkelsen, J. Gustafson, E. Lundgren
J. Phys. Chem. C. 119, 2572-2582, **2015**. DOI: 10.1021/jp511496w

Structure of the SnO_2(110)-(4×1) Surface

L. R. Merte, M. S. Jorgensen, K. Pussi,J. Gustafson, M. Shipilin, A. Schaefer, **C. Zhang** J. Rawle, C. Nicklin, G. Thornton, R. Lindsay, B. Hammer, E. Lundgren
Phys. Rev. Lett. 119, 096102, **2017**. DOI: 10.1103/PhysRevLett.119.096102

The Structure-Function Relationship for Alumina Supported Platinum During the Formation of Ammonia from Nitrogen Oxide and Hydrogen in the Presence of Oxygen

E. C. Adams, L. R. Merte, A. Hellman, M. Skoglundh, J. Gustafson, E. C. Bendixen, P. Gabrielsson, F. Bertram, J. Evertsson, **C. Zhang**, S. Carlson, P. A. Carlsson
Phys. Chem. Chem. Phys. 18, 10850, **2016**. DOI: 10.1039/c5cp07624b

Initial Oxidation of Cu(100) Studied by X-Ray Photo-electron Spectroscopy and Density Functional Theory Calculations

A.P. Borbon, B. Hagman, A. Schaefer, **C. Zhang**, M. Shipilin, A. Hellman, J. Gustafson, H. Grönbeck
Sur. Sci. 675, 64-69, **2018**. DOI:10.1016/j.susc.2018.04.015

Steps Control the Dissociation of CO_2 on Cu(100)

B. Hagman, A.P. borbon, A. Schaefer, L. R. Merte, M. Shipilin, **C. Zhang**, A. Hellman, E. Lundgren, H. Grönbeck, J. Gustafson
Submitted

Transient Structures of PdO During CO Oxidation Over Pd(100)

M. Shipilin, J. Gustafson, **C. Zhang**, L. R. Merte, A. Stierle, U. Hejral, U. Ruett, O. Gutowski, M. Skoglundh, P.-A. Carlsson, E. Lundgren
J. Phys. Chem. C 119(27), 15469-15476, **2015**. DOI: 10.1021/acs.jpcc.5b04400

Abbreviations

BCC	Body-Centered Cubic
CTR	Crystal Truncation Rod
DFT	Density Functional Theory
FCC	Face-Centered Cubic
(HE)SXRD	(High-Energy) Surface X-Ray Diffraction
IMFP	Inelastic Mean Free Path
LDOS	Local Density Of States
LEED	Low-Energy Electron Diffraction
SC	Simple Cubic
SR	Superstructure Rod
UHV	Ultra-High Vacuum
XPS	X-ray Photoelectron Spectroscopy
XRD	X-Ray Diffraction

Acknowledgments

2018, summer, many things have imprinted in my heart: the hottest summer ever in Sweden, and finally, I finished my Ph.D. thesis writing (with sweating). Many years passed, I gain a lot, not only the scientific knowledge but also the experiences that made me what I become, priceless!

I enjoy my life in Sljus, and there are many people I want to say thank from my deep heart! First of all, of course, my main supervisor Dr. **Johan Gustafson**. Thank you very much for teaching me knowledge, listening when I talked about my difficulties, guiding me with thoughtful discussion. You are always positive, never angry, kind to me, even though I keep challenging the border of your patient (I really did not want to). What you taught me are not only science but also the attitude of being a supervisor, so when I face a problem with my team, I always think twice if you were me what you would do. The knowledge and happy mood living style are also transferred from Prof. **Edvin Lundgren**, my co-supervisor. To be honest, I could not really get your sense of humor at the beginning of my Ph.D. Maybe I can complain because of the culture difference?! Or, maybe I just never thought about a professor can make a joke instantly, unexpected! Therefore, I feel so lucky that you are my supervisors.

I would like to thank **Sofie Yngman**, my super nice (both outside and inside) officemate, and you are another always positive person. A great listener, my consultant, my language teacher, my cafe labour,... we share sadness with tears, we encourage each other with words, we laugh together when we glad. I always saying:"Hey girl, you deserve better!".....

And **Patrik Wirgin**, very lovely, I like see your face-expression whenever you talk about something, so funny, you have such a power that makes people believes as you believed "who cares!". Happy all the time, this happy mood can affect people, and it's among our division, that's why I have such a good memory of these years in Sljus. I also want to thank the people who I discussed science with, such as Dr. **Uta Hejral**, Dr. **Zhe Ren**, Dr. **Gary Harlow**, **Benjamin Hagman** etc. Appreciate that! I had great time working with Dr. **Sara Blomberg**, Dr. **Natalia Martin**, Dr. **Mikhail Shipilin**, Dr. **Andreas Schaefer**, Dr. **Lindsay R. Merte**, Dr. **Alif Mohammad**, etc. Even though you all have left the division, but we were closely work for a while, quite appreciate for the time we spend time together. Many thanks to Dr. **Oliver Balmes**, Dr. **Anders Hellman**, Dr. **Per-Anders Carlsson** for the great collaboration.

Thanks to all the **synchrotron radiation facility** beamline people in world wide I have been, and also my **project founding groups**, and **all the col-**

leagues in div. of synchrotron radiation research.

I would like to thank all the people who supported me, such as **my friends**, **my families**. My mom **Xia Qu**, my dad **Tianjie Zhang**[1], my husband **Shenyuan Wang**, my daughter(s) (**Yufei Wang** and my business),....without you, I can not go this far and even will not be able to sit here and write this acknowledgement.....no, exclusive my business, without her, maybe I can complete my Ph.D. education earlier.

[1] in heaven

Contents

Chapter 1

Introduction

1.1 Background

Catalysts play an important role in our modern society. They are widely used in various fields, such as exhaust cleaning, pharmaceutical industry, and other chemical production industries [1–5]. By definition a catalyst promotes and controls a chemical reaction without being consumed by the reaction. Using a catalyst lowers the reaction energy barriers, compared to without the catalyst. Even though the function of catalysts have been studied for decades, fundamental understanding is still lacking to a large extent. Therefore, surface science research is used to obtain a better understanding of catalysis.

The benefit of using a catalyst is illustrated in Figure 1.1. Often a chemical reaction needs high energy to occur in gas phase, but the addition of a catalyst can promote it to occur faster and with less energy required. The catalyzed reaction is more complex, with at least adsorption and desorption as additional steps, but the reaction barrier of each step is significantly lower than for the uncatalyzed one. As an example from my studies, for CO oxidation, O_2 adsorbs dissociatively on the Rh surface into atomic O, while CO mainly adsorbs intact. CO can then react with atomic O and become CO_2, and leave the surface. Therefore, the high barrier of dissociating O_2 in gas phase is reduced.

A good catalyst should have an optimum interaction between the catalyst and the reactants. If the reactants are too weakly bound, the catalyst cannot activate the reactants for the catalytic reaction. If the reactants are too strongly bound, they will not be able to react with each other. Therefore, the reactants should bind well enough to activate them but not too hard to allow them to react

further, as descried by the Sabatier principle [6]. The Pt-group metals have proved to have the right reactivity for many reactions. For example, for the CO oxidation reaction, the Pt-group metals are reactive enough to dissociate O_2, but not CO, and inert enough for CO and O_2 to react to form CO_2 that desorbs.

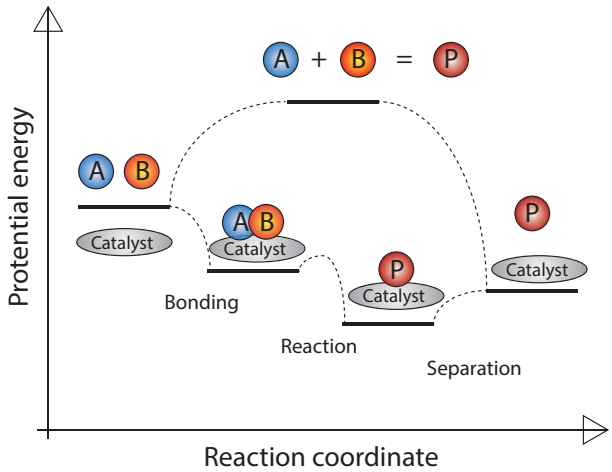

Figure 1.1: Energy diagram of a chemical reaction occurring with and without a catalyst. Without the catalyst, the reaction requires high energy in order to proceed from reactants (A and B) to the product (P). However, when the reactants adsorb on a catalyst, they become activated and the energy barriers for the reaction are lower than for the uncatalyzed reaction. At the end, the product P separates from the catalyst. Overall, the rate of the catalytic reaction is much higher and the activation energy is significantly lower than that of the uncatalyzed one [7].

The Pt-group metals are, however, very expensive and in order to use them as efficient as possible and minimize the quantity used, it is desirable to maximize the surface area and create as many active sites as possible. Hence, industrial catalysts usually consist of nanoparticles dispersed in a porous oxide support. They also work in atmospheric or higher gas pressures. This makes it difficult to study the surface of the active nanoparticles, which has an essential role in catalytic reactions. In addition, these nanoparticles expose different facets, separated by steps and kinks, as illustrated in Figure 1.2 [8–11]. In order to be able to study catalytic surfaces, scientists typically use model catalysts consisting of perfect low-index single crystals and investigate them under ultra high vacuum (UHV) conditions. These differences, between the industrial and laboratory conditions, are called the **material gap** and the **pressure gap**. In order to link surface science to industrial catalysis, I try to bridge these gaps by identifying important structures on more complex model systems at higher pressures, in conjunction with detailed investigations of their reaction mechanisms at lower pressures and theoretical simulations.

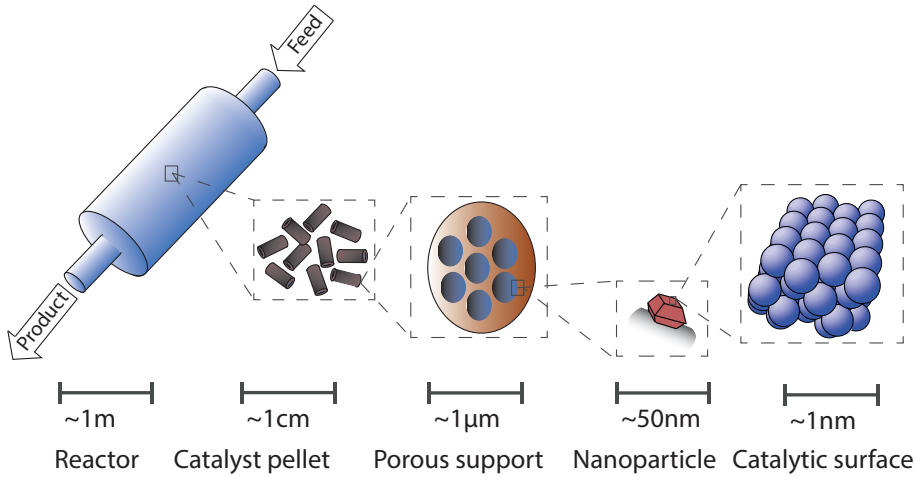

Figure 1.2: Illustration of the different components in an industrial catalyst, demostrating the material complexity.

1.2 This work

The projects that I have been working with are mainly aimed at finding the relation between the surface structure and the catalytic activity, so that a structure-function relationship can be established and a deeper understanding can be obtained. Especially, I have studied CO oxiation over vicinal, or stepped, as well as oxidized Rh and Pd surfaces, and followed how the surface structure and catalytic activity changed with experimental conditions, such as gas mixture, pressure and temperature. This has been done from UHV to close to atmospheric pressures using X-ray Photoelectron Spectroscopy (XPS) and Surface X-Ray Diffraction (SXRD) in combination with mass spectrometry (MS). In addition, Density Functional Theory (DFT) calculations, done in collaboration with the Competence Centre for Catalysis at Chalmers University of Technology, has played a crucial role for the interpretation of the experimental results.

This thesis consists of an introduction to the field, followed by a number of papers, where the results are reported. In **Paper I** and **Paper IV**, the vicinal Rh(553) and Pd(553) surfaces are studied during CO oxidation under realistic condition using SXRD, and certain metallic as well as oxidized surface structures are identified as being essential for understanding the catalytic activity. The identified metallic Rh structures are then studied in detail at low pressures, using XPS, in **Paper II** and **Paper III**. The importance of the surface structures of the oxides formed are studied in **Paper V**, where it is shown that the certain Pd

oxides are at least as active as the metallic surface, while Rh oxides are inactive. Finally, in **Paper VI**, the use of very high energy X-rays, in combination with a large 2D detector for Surface X-ray Diffraction is demonstrated as a powerful tool for *in-situ* studies of model catalysts under harsh condistions.

Chapter 2

Surfaces

Most materials, including most metals, are crystalline. This property is crucial for the behaviour of the materials, and in this chapter, I will introduce crystal structures in general and surface structures in particular. I will discuss more or less simple structures, from flat low-index surfaces to vicinal surfaces with a high density of steps.

2.1 Crystal structure

A crystal consists of a periodic arrangement of atoms, which gives a crystalline structures. The crystal structure is described by a lattice, where each lattice point is connected to one or a group of atoms. The lattice is defined such that a general lattice vector

$$R_n = n_1\mathbf{a_1} + n_2\mathbf{a_2} + n_3\mathbf{a_3} \tag{2.1}$$

Here, n_1, n_2 and n_3 are integers and $\mathbf{a}_1$, $\mathbf{a}_2$ and $\mathbf{a}_3$ are the lattice basis vectors.

The simplest structure is the simple cubic (SC) structure, which has one atoms located at each corner of the cubic unit cell, as shown in Figure 2.1 (a). The repeated set of atoms are called the **unit cell**.

Most metals have one of four common structures, namely the SC, face-centered-cubic (FCC), body-centered-cubic (BCC) and hexagonally close-packed (HCP) structures shown in Figure 2.1 [12]. BCC and FCC are similar to the SC structure with extra atoms either located at the center of the cube or on the center

of each face. Viewed along the diaglonal of the cube, the FCC structure is built up by close packed hexagonal layers, similar to the HCP structure.

I have worked with Rh and Pd, which both have the FCC structure. Hence, the following discussion will focus on this structure.

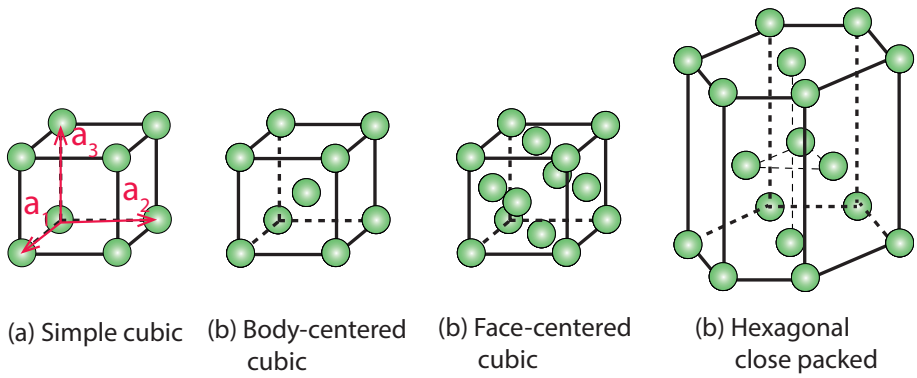

Figure 2.1: Model of structures for (a) the Simple Cubic (SC) with stacking of *abca*, (b) the Body-centered cubic (BCC), which has an atom in the center of the cubic, (c) the Face-centered cubic (FCC) , which additional atoms locate at center of each face and (d) the Hexagonal close packed (HCP).

2.2 Crystal surface

A surface is created by slicing the bulk structure, as shown in figure 2.1, along a specific plane. Depending on the orientation of this plane, different surface structures are obtained, as discussed in section 2.2.1. Creating surfaces includes breaking of inter-atomic bonds, and hence increases the energy of the system. The energy needed to break the bonds is the surface energy, typically given per unit area, and determines the stability of the surface. This will be discussed in section 2.2.2

2.2.1 Surface structure and Miller index

The orientation of different crystallographic planes are denoted by the so-called **Miller indices**. The Miller indices is a set of three integers $(h\ k\ l)$ given by the reciprocal of the x, y and z coordinates of the intersections between the plane and the corresponding axes defining the lattice. To illustrate this, Figure 2.2 shows a 2D version of a crystal structure with three different lines. The orientation for these lines are denoted as the reciprocal value of the intersection of both axes. For example, line (a), intersects both axes at 1. Hence, the line

can be denoted as $(1/1 \quad 1/1) = (1 \quad 1)$. Line (c), intersects the x- axis in 1 but is paralell to the y- axis, which can be viewed as intersecting in infinity. This line can then be denoted as $(1/1 \quad 1/\infty) = (1 \quad 0)$. Line (b), intersects the x-axis at 1, and the y-axis at 2, yielding the reciprocal values $(1 \quad 1/2)$. For convenience, this is normalized to lowest possible integer values, in this case by multiplication with 2, and the corrected Miller index is (2 1).

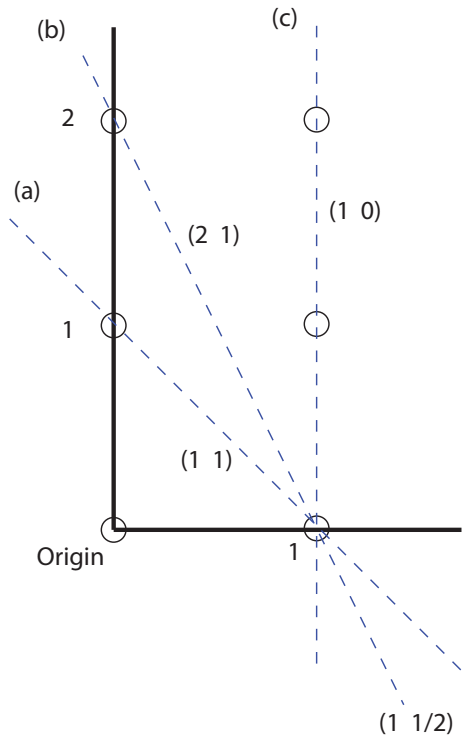

Figure 2.2: Miller index calculation in 2D plot. The orientation for these dashed lines are denoted as the reciprocal value of the intersection of both axes. Line (a)-(c) represent (1 1), (2 1) and (1 0).

The same rule applies to 3D structures, as shown in Figure 2.3 for the (100), (110) and (111) planes of FCC crystals.

It is worth noting that several miller indices, such as (100), (010) and (001) in the case of cubic structures, result in equivalent surface structures. To denote any of these, one often uses curly brackets instead, such as {100}. Square brackets are used for specifying a certain direction. For instance, the [100] direction is paralell to the x axis. Note that the $[hkl]$ direction is perpendicular to the (hkl) plane.

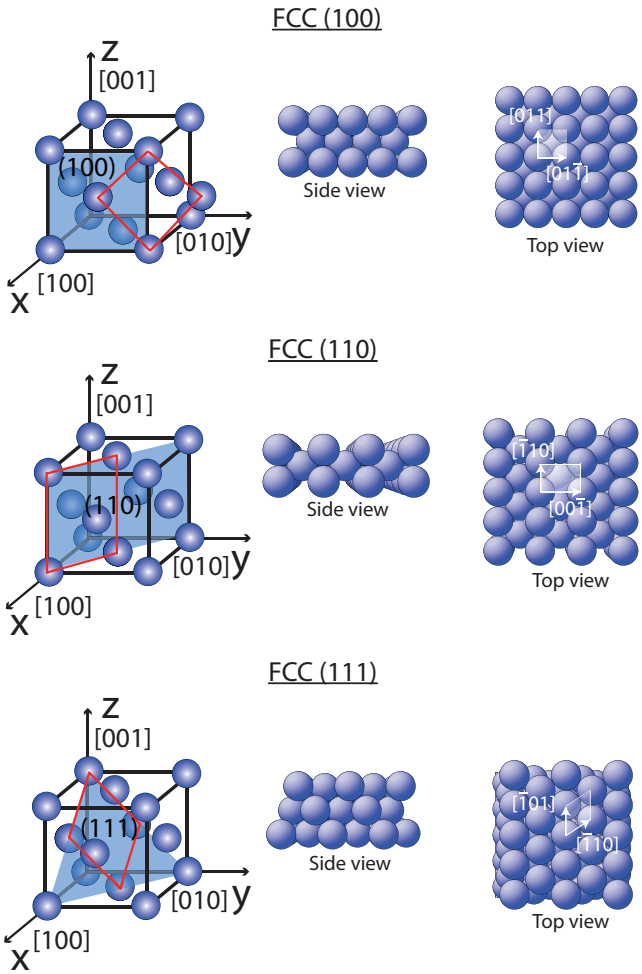

Figure 2.3: Model of the FCC unit cell with the (100), (110) and (111) surfaces indicated and shown in side and top views. In the left panel, a FCC cubic structure is shown with a corner atom as origin for the x, y and z coordination axes. The dark blue area represents the plane for (100), (110) and (111), respectively. The red marker indicate the planes.

2.2.2 Surface Energy

The structure of a crystal is determined by the interatomic bonds, which are optimized such that the energy is minimized. When a surface is created, some of these bonds are broken and the energy is increased. This increase is defined as the surface energy. The surface energy in turn determines the stability of

different surface orientations, as well as the reactivity of the surface.

Most important for the surface energy is the number of interatomic bonds that are broken in the creation of the surface. In the bulk of an FCC structure, all atoms have 12 nearest neighbours. As seen in Figure 2.3, atoms in the (100) surface have four nearest neighbours in the surface plane, and another four in the second layer, yielding a total of eight nearest neighbours. Correspondingly the (110) surface atoms have seven nearest neighbours, while the (111) surface atoms have nine nearest neighbours. Hence, the atoms in the (111) surface only misses three bonds relative to the atoms in the bulk, making these more satisfied than the ones on (100) and (110) surfaces.

On the other hand, the atoms are more densely packed on the (111) surface and in order to say anything about the stability of the surface, the number of broken bonds has to be counted per surface area. Using the simple square unit cell of the (100) surface as unit area, the area per atom is 0.87 a^2, 1 a^2 and 1.4 a^2 for the (111), (100) and (110) surfaces, respectively. The corresponding number of broken atomic bonds per unit area is 3.5 bonds/a^2, 4 bonds/a^2 and 4.2 bonds/a^2. Hence, the (111) surface is the most stable of these surfaces, followed by (100) and (110).

Although this is a fairly good approximation, it is important to point out that the surface energy is not perfectly proportional to the number of broken bonds. Hence, the stability of the different surface orientations varies between different materials.

The bonds that are broken during creation of a surface can be compensated by bonds to other atoms and molecules, such as the reactants of a catalytic reaction. This can then change the stability of different structures and result in adsorbate induced reconstructions which will be discussed further in the next chapter.

2.2.3 Low index and vicinal surface

As described earlier in this chapter, low-index surfaces, that is surfaces cut along planes with h, k and l being 0 or 1, typically rather stable. In contrast, a high-index or vicinal surface exposes a periodic array of steps separated by low-index terraces [13–16]. A real surface is never perfect but will expose a certain degree of defects. The step is one type of defect which exist in most surfaces and influence the surface catalytic activity and reactivity [13, 14]. The flat (100) and (111) as well as the vicinal (553) surfaces of Rh and Pd were studied in

this thesis. The (553) surface consists of periodic array of five atoms wide (111) terraces separated by steps exposing $(11\bar{1})$ [1] microfacets as shown in Fig 2.4.

One of the aims of the work in this thesis is to study how the steps affect the catalytic CO oxidation activity. This has been done by comparing the activity of low-index and vicinal surfaces, and especially connected that to the surface structure. In **Paper II**, the results show that the vicinal Rh(553) surface is indeed more active for CO oxidation than Rh(111). The active site is, however, found not to be the step, but rather the terrace close to the step. The reason for the higher activity is relaxation of the atomic structure instead of lower coordination.

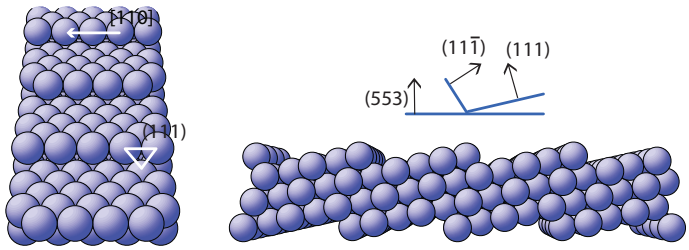

Figure 2.4: Model of a (553) surface from (A) top view and (B) side view. The (553) surface is a vicinal surface with periodical steps. It consists of 5 atoms wide (111) terraces, separated by $(11\bar{1})$ microsteps.

[1] For convenience, minus signs in miller indices are usually placed above the index, such that $\bar{1} = -1$.

Chapter 3

Gas-Surface Interaction

When a surface is exposed to a gas, the gas molecules tend to stick to the surface in order to minimize the total energy. This process is called adsorption and will result in a compensation of the bonds that were broken in order to create the surface as well as in a general change in the structure and stability of both the surface and the molecules. For instance, molecules may dissociate, the surface may reconstruct and new materials, such as oxides, may form [17–19]. Adsorption is the first step in catalytic reactions.

This chapter will introduce adsorption using CO and O_2 on Rh(111) and Rh(553) as the main examples. We will see how these molecules adsorb on the unreconstructed surface at low exposures, while a higher coverage of adsorbates (the adsorbing molecules) may lead to a reconstruction of the substrate surface or, in the case of oxygen, to oxide formation.

3.1 Adsorption

Adsorption is divided in two categories; weak physisorption based on van der Waals forces and hydrogen bonds, and the stronger chemisorption, where the electronic structure is changed in covalent bonds. For catalytic reactions, changes in electronic structure and stability is of major importance, so chemisorption is in focus in this thesis.

3.1.1 Adsorption sites

The initial adsorption, especially at relatively low temperatures, typically leaves the substrate structure close to unaffected, while the adsorbates stick to the surface. Due to symmetry, molecules will usually adsorb in symmetric adsorption sites. On the low-index surfaces of an FCC crystal, these are on top, bridge, three-fold hollow (3fh) and four-fold hollow (4fh), as shown in Figure 3.1. For the 3fh sites on the (111) surface, there are two different possibilities depending on the position relative to the atoms in the second substrate layer. If there is a atom right below in the second layer, the site is denoted hcp, due to the similarity to the *aba* stacking of the hexagonal planes in the hcp crystal structure. Similarly, if there is no atom right below in the second layer, this is an fcc site, due to the *abca* stacking in the fcc crystal structure. On the (110) surface, there are also two different bridge sites, short or long as described in Figure 3.1. As the coverage increases, the adsorbates will form ordered structures due to the usually repulsive interaction between adsorbates.

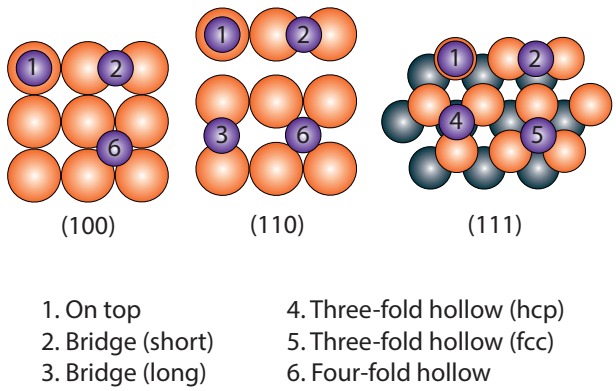

Figure 3.1: Model of different adsorption sites on (100), (110) and (111). The diffference between fcc and hcp hollow sites are whether the position of the adsorbate conincides with an atom in the second layer of the substrate.

3.1.2 Adsorption Structures

When the coverage increases, the adsorbates tend to organize in well-ordered periodic structures, which most often are described using the so-called **Wood's notation** [20]. It relates the basis vectors of the overlayer unit cell to those of the substrate according to

$$\mathrm{M}(hkl)x(\frac{|\mathbf{a_1'}|}{|\mathbf{a_1}|} \times \frac{|\mathbf{a_2'}|}{|\mathbf{a_2}|}) - R\alpha^\circ - n\mathrm{A} \tag{3.1}$$

where, M(hkl) is the element and miller index of the substrate surface, x is either p or c denoting whether the unit cell is primitive or centered, respectively, $\mathbf{a_1'}$ and $\mathbf{a_2'}$ are the magnitude of the overlayer basis vectors, $\mathbf{a_1}$ and $\mathbf{a_2}$ are the magnitude of the substrate basis vectors, α° is the angle between substrate and overlayer unit cells and nA is the number per unit cell and chemical species of the overlayer molecules or atoms. The notation include information on the size of the unit cell, orientation of the structure and adsorbate coverage.

Figure 3.2 shows examples of overlayer structures on a fcc(100) substrate surface. The blue and red balls represent the substrate and the adsorbate atoms, respectively. The primitive adsorbate structure in Figure 3.2 A has one basis vector that is twice as long as that of the substrate, while the other is of the same length. Hence, this is a $p(2 \times 1)$ structure. Further the basis vectors of the overlayer are parallel to those of the substrate, that is, the relative rotation is 0°. Finally, there is one adsorbate per unit cell and the full Wood's notation would be M(100)$p(2 \times 1) - R0^\circ - 1$A. Most often, some of this information is implied, and therefore omitted. The structure in Figure 3.2 A would then be a (2×1) structure.

The primitive unit cell of the structure in 3.2 B has unit vectors that are $\sqrt{2}$ times those of the substrate and rotated 45°, yielding a $p(\sqrt{2} \times \sqrt{2})R45^\circ$. Since it is often more convenient to use a unit cell that is not rotated relative to the substrate, this is instead often denoted as $c(2 \times 2)$, that is a (2×2) structure with an extra lattice point in the center of each unit cell.

An alternative and more general notation is the so-called **matrix notation**, which describes the size and orientation of the overlayer unit cell relative to that of the substrate according to the matrix $\begin{pmatrix} G_{11} & G_{12} \\ G_{21} & G_{22} \end{pmatrix}$ defined as

$$\mathbf{a_1'} = G_{11}\mathbf{a_1} + G_{12}\mathbf{a_2} \tag{3.2}$$

$$\mathbf{a_2'} = G_{21}\mathbf{a_1} + G_{22}\mathbf{a_2} \tag{3.3}$$

$$\begin{pmatrix} \mathbf{a_1'} \\ \mathbf{a_2'} \end{pmatrix} = \begin{pmatrix} G_{11} & G_{12} \\ G_{21} & G_{22} \end{pmatrix} \begin{pmatrix} \mathbf{a_1} \\ \mathbf{a_2} \end{pmatrix} \tag{3.4}$$

For the structure in Fig 3.2A, this yields

$$|\mathbf{a_1'}| = 2|\mathbf{a_1}| + 0|\mathbf{a_2}| \tag{3.5}$$

$$|\mathbf{a_2'}| = 0|\mathbf{a_1}| + 1|\mathbf{a_2'}| \tag{3.6}$$

and the matrix notation would be $\begin{pmatrix} 2 & 0 \\ 0 & 1 \end{pmatrix}$.

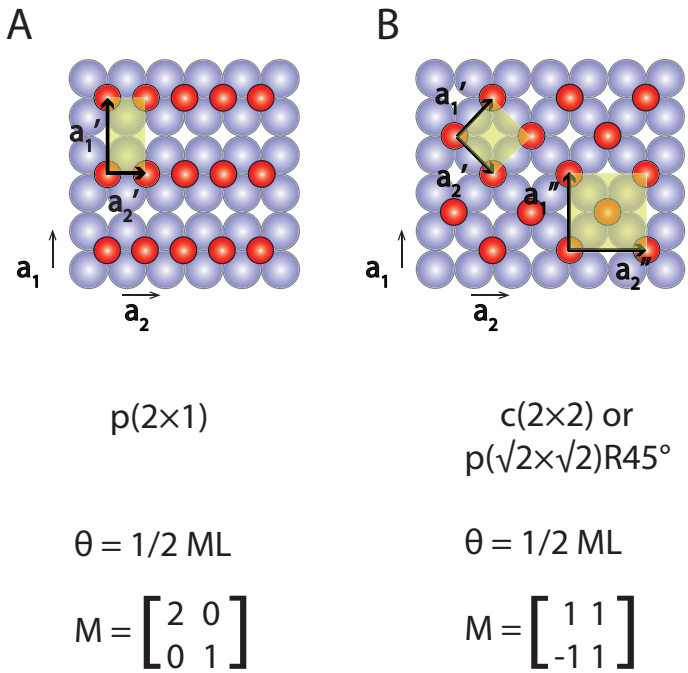

Figure 3.2: Two examples of adsorption structures on a fcc(100) surface, with their Wood's and matrix notations.

3.1.2.1 CO and O Adsorption on Rh(111)

When O adsorbs on Rh(111), it dissociates into single atoms that prefer to adsorb in 3fh-fcc sites. As the coverage reaches 1/4 monolayers (ML), where 1 ML means that the same number of atoms are adsorbed as there are atoms in the surface layer of the substrate, the ordered (2×2) structure is formed [21–27], as shown in Figure 3.3(a). Figure 3.3(b-d) shows the (2×1), $(2\sqrt{3}\times2\sqrt{3})R30°$ and (2×2)-3O structures that form when the coverage increases further up to the saturation coverage of 3/4 ML. At this point, further exposure to O_2 does not lead to adsorption. In the $(2\sqrt{3}\times2\sqrt{3})R30°$ structure, O adsorbs not only in fcc sites but also in hcp sites, as indicated in the figure by red and orange balls.

Figure 3.4 shows CO adsorption on Rh(111) surface . In contrast to O, CO prefers to adsorb in on-top sites, forming (2×2), $(\sqrt{3}\times\sqrt{3})R30°$ and (2×1) structures at 1/4, 1/3 and 1/2 ML coverage respectively. At this point, it

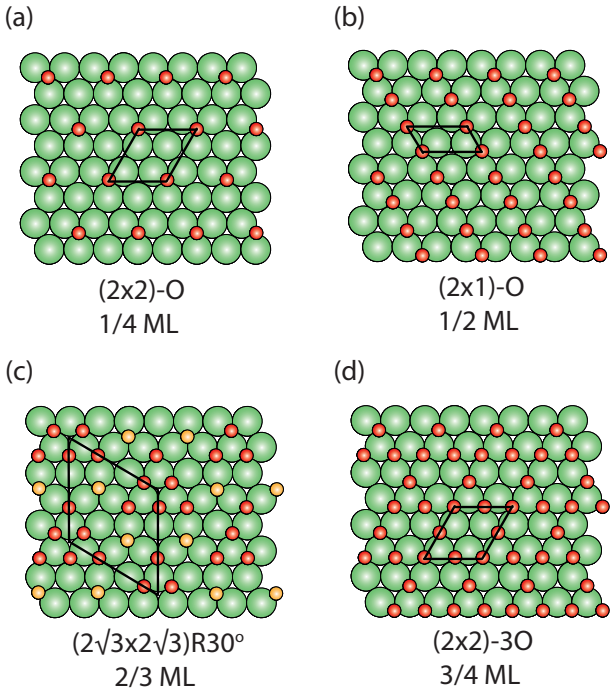

Figure 3.3: Model of O adsorption on Rh(111) with increasing coverage. Green balls are Rh atoms, red balls are O atoms on fcc hollow sites, orange balls are O atoms on hcp hollow sites.

becomes unfavourable to add more CO in on top sites, as the local coverage would be too high. Instead some of the CO molecules move to 3fh sites, and at the saturation coverage of 3/4 ML, we again find a (2×2) structure with three molecules per unit cell; one on-top, and two in 3fh sites (one fcc and one hcp site), as shown in Figure 3.4(e). [21–23, 28–35].

The adsorbate structures of CO on Rh and Pd efficiently blocks the dissociative adsorption of O_2, which makes these CO covered surfaces show low activity. Since CO adsorption is associative, however, O precovered surfaces allows for CO adsorption, resulting in coadsorption structures that enables the CO oxidation reaction. These coadsorption structures on Rh(111) were studied by Schwegemann *et al.* [21, 36] and Jaworowski *et al.* [24] at temperatures below the activation energy for the reaction, and are summarized in Figure 3.5. Starting with a (2×2) structure of O with a coverage of 1/2 ML, there is one Rh atom in each unit cell that is not coordinated to O. This is where CO starts to adsorb in the (2×2)-O+CO structure shown in Figure 3.5 a. For further CO adsorption, there are no available on-top sites, and as with only CO, we find a (2×2)-O+2CO structure with CO in both on-top and 3fh sites as shown in Figure 3.5 b. Finally, starting with the (2×1)-O structure with a higher oxygen

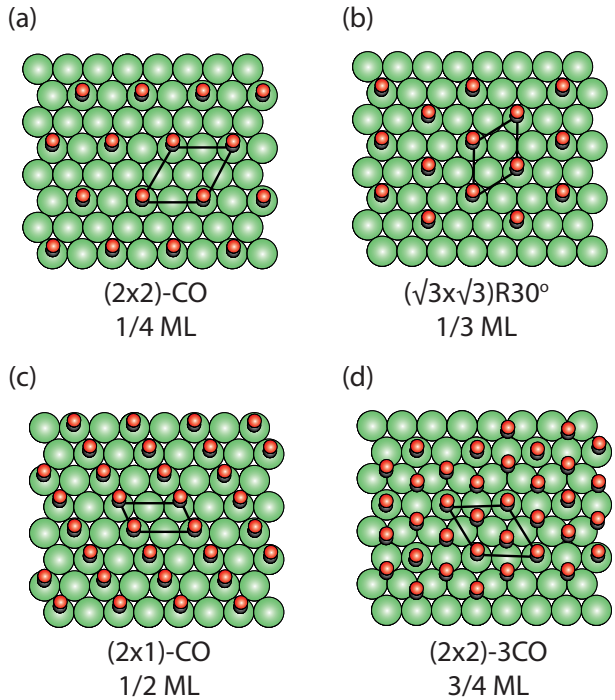

Figure 3.4: Model of CO adsorption on Rh(111) with increasing. Green balls are Rh atoms, red balls are O atoms on fcc hollow sites. (a) at 1/4 ML, the structure is (2×2) - CO.(b) at 1/3 ML, the structure is $(\sqrt{3} \times \sqrt{3})R30°$. (c) at 1/2 ML, the structure is (2×1) - CO. (d) at 3/4 ML, the structure is (2×2) - 3CO.

coverage of 1/2 ML, the adsorbing CO pushes half of the O atoms from the 3fh-fcc to 3fh-hcp sites, hence making the on-top sites available for the formation of a $(2 \times 2) - 2O + CO$ structure as shown in Figure 3.5 c. In **Paper III**, we find that at a sample temperature of -180° C, this change of oxygen site cannot occur, and the CO initially adsorbs in 3fh sites. Upon heating, however, we find that a rearrangement to the structure in Figure 3.5 c, before the CO oxidation reaction starts.

3.2 Oxides

In nature, most metals are found in the form of oxides, and if exposed to high enough O_2 pressures at high enough temperature for the atoms to mix, also Rh and Pd will oxidize. This drastically changes the interaction with the surrounding and especially the catalytic properties. Historically, it has been found that oxides in general are rather inactive for CO oxidation. More recently, however, it has been suggested that the oxide phases are responsible for the high CO

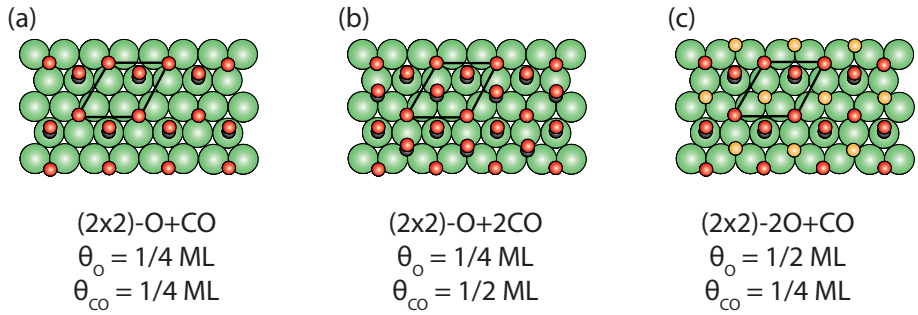

Figure 3.5: Model of O and CO co-adsorption on Rh(111).

oxidation activity over Rh, Pd, Pt, and Ru. This has been under debate for almost two decades, but in **Paper V** we show that Pd oxides can be active while Rh oxides are inactive. The determining factor is the surface structure, which will be discussed for different Pd and Rh oxide structures in this section.

3.2.1 Palladium oxide

A PdO bulk oxide unit cell is shown in Figure 3.6 A, where the green (100) plane is the stable surface orientation for pure PdO [37–40]. Here, all the Pd atoms, in the bulk as well as on the surface, are coordinatively saturated, binding to four O atoms as shown in Figure 3.6 B. When oxidizing a Pd crystal however, first a surface oxide with a single PdO(101) layer (the yellow plane) is formed, as shown in Figure 3.6 C. In this surface, half of the Pd atoms are coordinatively saturated, while the other half are Coordinatively UnSaturated (CUS), only binding to two O atoms. The presence of the metal underneath the oxide film stabilizes the (101) surface instead of (100) [37–39]. This is the case also for thin bulk oxide films, which thus expose the (101) surface as shown in Figure 3.6 D. In this case the CUS atoms are also coordinated to O in the second layer, and bind to three O atoms. If the oxide film grows thick, the stabilization stops and the (100) surface is exposed. At the same time the connection to the substrate is broken and the oxide becomes polycrystalline.

Concerning the activity for catalytic CO oxidation, CO does not bind strong enough to the surface with only fully saturated Pd atoms. Consequently, the thick bulk oxide is not very active. The CUS atoms on the surface oxide and thin bulk oxide are, however, able to adsorb CO, and in **Paper V** we show that these oxides are at least as active as the metallic surface.

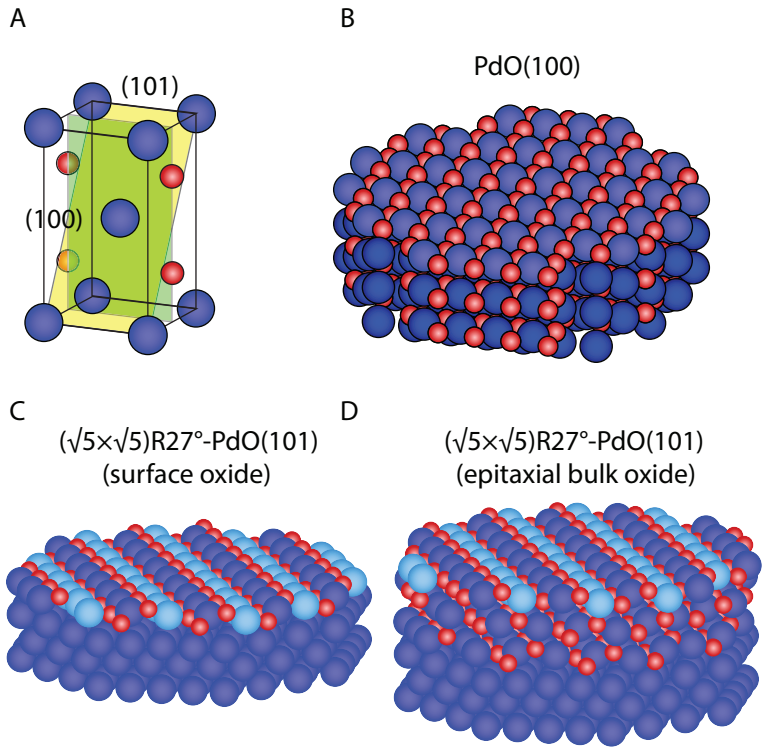

Figure 3.6: Models of PdO. A. The unit cell of PdO. The yellow and green planes represent (101) and (100) surface orientations. B. PdO (100) bulk structure, with each Pd atom coordinated to four O atoms. C. $(\sqrt{5}\times\sqrt{5})R27^\circ$ - PdO(101), which is a surface thin oxide. It is a trilayer O-Pd-O structure, where the Pd atom bind 2 and 4 O atoms [41, 42]. When the surface oxide grows thicker, it becomes an epitaxial bulk oxide with Coordinatively UnSaturated (CUS) Pd atoms (denoted as the light blue color balls) as shown in D.

3.2.2 Rhodium oxide

For Rh, the unit cell of the bulk oxide, Rh_2O_3, is shown in Fig 3.7 A, with a hexagonal structure with complex stacking order. The stable surface of this oxide is completely O terminated [43, 44], and does not bind CO very well. This is also the case for the surface oxide, which consists of a trilayer with three hexagonal O-Rh-O layers as shown in Figure 3.7 B [45–48]. In **Paper V** we show that the Rh oxides are, indeed, not very active for CO oxidation.

The very initial oxidation of Rh(110), however, results in a 1D oxide with a (10×2) missing-row structure as shown in Figure 3.7 C [49–52]. Along the remaining rows, two out of ten Rh atoms are removed, and the remaining eight are stretched out over nine lattice distances, and surrounded by 4 O atoms each. The same structure can be found on Rh(331) facets [53], as well as on surface with (100) steps [54]. In **Paper III** we find that this 1D oxide, in contrast

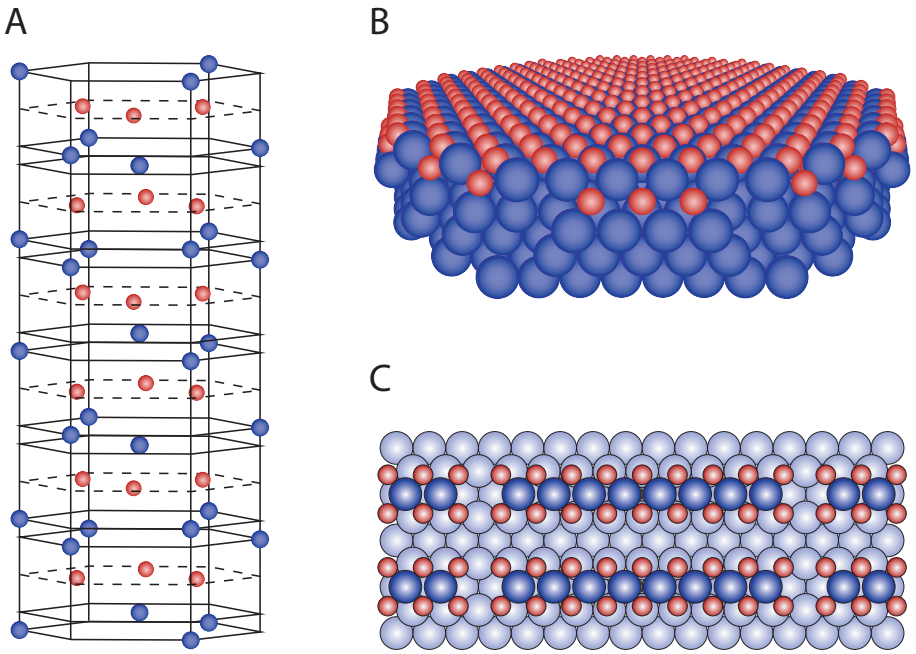

Figure 3.7: Models of Rh oxides: (A) Bulk Rh_2O_3 unit cell, (B) (9×9) surface oxide on Rh(111) and (C) 1D oxide on Rh(110), which consists of a (10×2) missing-row structure.

to the other Rh oxides, is highly active for CO oxidation, probably due to CO being able to adsorb on the narrow (111) terraces separating the steps.

3.2.3 Surface reconstruction and faceting

As mentioned above, the formation of adsorption structures or oxides changes the energy and hence the stability of a surface. Especially, the relative stability of different surface structures may change, resulting in a reconstruction of the surface layers [55]. For instance, during the formation of the 1D oxide on Rh(110), every second surface row is removed in what is called a missing row reconstruction [56]. Another nice example of reconstructions can be seen when Rh(553) is exposed to O_2 [53] or reaction mixtures of CO and O_2, as discussed in **Paper I**.

After exposing the Rh(553) surface to a CO-rich CO+O_2 gas mixture, at temperatures where the catalytic activity is high, the steps move closer together in (110) facets, as indicated by the green atoms in Figure 3.8, while the (111) facets (yellow) grows such that the macroscopic orientation of the surface is unchanged. The driving force for this faceting is probably that as much CO as possible shall

be able to adsorb. The CO prefers to adsorb on steps, since the step atoms, as discussed in Chapter 2, are most undercoordinated and hence most reactive. The faceting, however, does not increase the number of steps, so the adsorption on the steps cannot be the driving force. Instead, the extended (111) terraces can probably accommodate more CO than when regularly interupted by steps, which means that the energy is lower for the facetted surface than the original orientation.

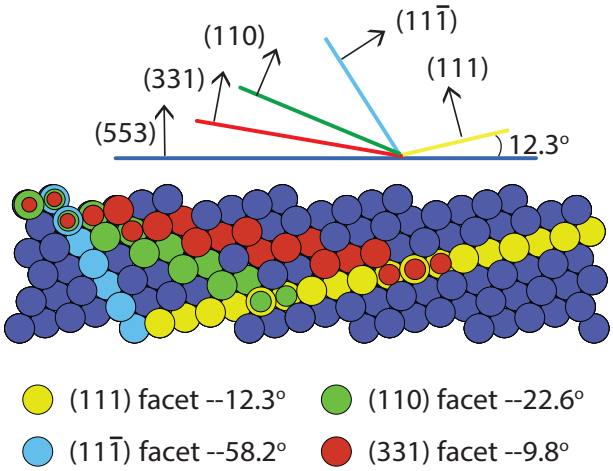

Figure 3.8: Model of vicinal (553) surface with different facets. The facets are (111) (yellow), (11$\bar{1}$) (light blue), (110) (green) and (331) (red). The angles to the normal (553) surface is indicated for each facets, respectively. In order to keep the macroscopic surface orientation unchanged, the shorter terraces of the new facets are compensated by larger (111) facets.

In a stoichiometric reaction mixture, with this high reaction rate, the coverage of both CO and O will be very low, and the surface will return to the original (553) orientation, as shown by the dark blue atoms.

In a slight oxygen excess, the 1D oxide will form along the step edges. Again, the remaining (111) terraces will not be able to accommodate as much adsorbates as extended (111) terraces. Hence, the steps will again be pushed closed together, but the 1D-oxide needs more space than the adsorbed CO, and the result is (331) facets (red). Note that this is slightly denser than for the 1D oxide on Rh(110).

Finally, in an even more oxygen rich gas mixture, the surface oxide forms on the (111) terraces, which means that these grow further together with equivalent (11$\bar{1}$) facets, as shown by the light blue atoms.

Chapter 4

Catalysis

A chemical reaction happens when molecules or atoms of the reactants collide, break internal bonds and create new bonds forming the products. The breaking and creation of bonds typically requires a certain energy, which is referred to the activation energy of the reaction. The role of a catalyst is to provide an alternative path for the reaction, where intermediate bonds are made between the reactants and the surface of the catalyst. In this way, the reaction is divided into several steps, but the involved energy barriers are lower, such that the reaction proceeds faster. This chapter will discuss reaction rates, their dependence on activation energies and temperature, and how this applies to catalysis.

4.1 Reaction Kinetics

The rate of a reaction expresses how many product molecules are formed, and reactant molecules are consumed, during a certain time. For non-catalyzed reactions where the reactants are mixed in gas or liquid phase and directly react to the product, the rate is usually expressed in terms of the concentration of reactants and products over time. For instance, for a reaction described by the simple stoichiometry condition

$$aA + bB \Rightarrow cC \tag{4.1}$$

the rate expresses how fast the concentration changes according to

$$Rate = -\frac{1}{a}\frac{d[A]}{dt} = -\frac{1}{b}\frac{d[B]}{dt} = \frac{1}{c}\frac{d[C]}{dt} \tag{4.2}$$

where d[A], d[B] and d[C] are the changes in concentration of reactants (A and B) or product (C) over a time period dt and a, b and c are the stoichiometry coefficients. Note that the negative sign corresponds to a negative change of a reactant concentration, since the reactant is consumed. On the other hand, the product results in a positive sign. Such an expression for the rate of a reaction is called a **rate law** [57].

The rate of a reaction varies with the concentration of reactants according to

$$Rate = k[A]^x[B]^y \tag{4.3}$$

where, k is the so-called rate constant, and x and y are the order of the reaction relative to the reactants A and B, respectively, and relates how the rate changes with the concentration. For example, if $x = 1$ the reaction rate increases linearly with the concentration of A. If the $x = 0$, the rate does not depend on the concentration of A, and if $x < 0$ the rate drops with increasing concentration of A.

Usually, the higher temperature, the higher reaction rate. This behaviour is described by the empirical Arrhenius equation, that describes how the rate constant, despite of the name, varies with temperature and activation energy:

$$k(T) = Ae^{-E_a/k_BT} \tag{4.4}$$

Here, A is a pre-exponential factor, E_a is the activation energy, or the reaction barrier, which describes the minimum energy required for the reaction to occur, k_B is the Boltzmann constant [7], and T is the temperature. From this expression it is directly clear that the reaction rate, which at a certain concentration of reactants is proportional to the rate constant, increases exponentially with the temperature. Similarly, the Arrhenius equation says that the reaction rate increases exponentially with decreased activation energy, which is the most important aspect of the Arrhenius equation when it comes to catalysis, as discussed further below.

For a gas phase reaction, the Arrhenius equation can be explained by the Maxwell-Boltzmann distribution, which describes the distribution of kinetic energies among gas-phase molecules and hence the available energy in collisions between these particles. The Maxwell-Boltzmann distribution is described by

$$f(E) = 2\sqrt{\frac{E}{\pi}}\left(\frac{1}{k_B T}\right)^{3/2} e^{-\frac{E}{k_B T}} \tag{4.5}$$

where the first part describes how the number of states varies with the kinetic energy, and the second part is the Boltzmann distribution describing to what extent these states are filled depending on the temperature. Figure 4.1 shows the Maxwell-Boltzmann distribution curve at three different temperatures. The striped area underneath the curve of temperature T_3 and above the activation energy $E_{a,1}$ corresponds to the number of collisions with high enough energy to overcome this activation energy, such that they can lead to reaction at this temperature. This area, and hence the reaction rate, increases significantly if the activation energy is decreased to $E_{a,2}$ and decreases if the temperature is lowered to T_2 or T_1. As seen in Equation 4.5, the dependences of the Maxwell-Boltzmann distribution on temperature and kinetic energy are not strictly exponential but at higher energies, in which range relevant activation energies usually lie, the exponential term completely dominates. Hence the empiric Arrhenius equation shows an exponential dependence, while the non-exponential terms contribute to the prefactor.

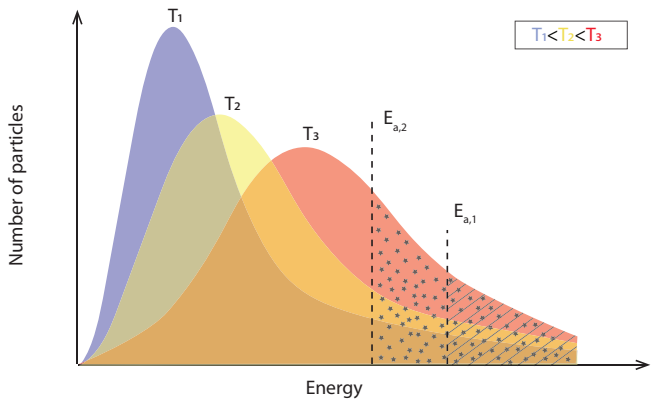

Figure 4.1: The Maxwell-Boltzmann distribution curve for three different temperatures, describing the distribution of kinetic energies among gas-phase molecules and the available energy in collisions between these particles. The collisions with energy above E_a. may lead to reaction.

In order to experimentally determine the activation energy of a reaction, it is useful to express the Arrhenius equation on a logarithmic form:

$$\ln k(T) = -\frac{E_a}{k_B}\frac{1}{T} + \ln A \tag{4.6}$$

This shows that if the reaction rate is measured at different temperatures and plotted logarithmically against the inverse temperature, the result is a linear plot

where the slope is directly given by the activation energy as shown in Figure 4.2.

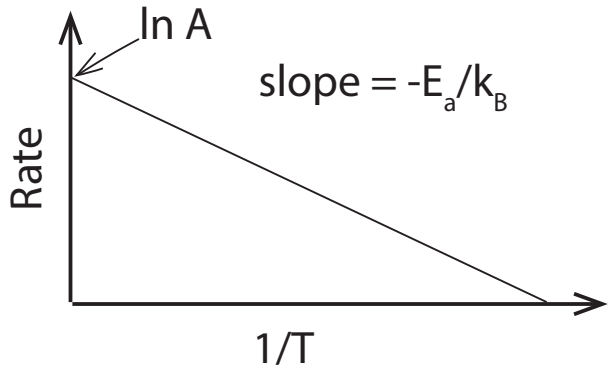

Figure 4.2: Arrhenius plot. The logarithm of a reaction rate plotted against inverse temperature. The slope gives the activation energy.

4.2 Heterogeneous catalysis

Catalysis can be classified into heterogeneous catalysis, where the catalyst and reactants are in different phases, and homogeneous catalysis, where the catalyst and reactants are in the same phase [9]. This thesis focuses on heterogeneous catalysis with solid catalysts and gaseous reactants. More specifically, I have studied catalytic oxidation of CO over the surface of noble metals. This catalysis is essential, for instance, for cleaning of automotive exhaust gases.

Figure 4.3 schematically describes the CO oxidation process over a transition metal single crystal. The reactants are initially in gas phase but adsorb on the catalytic surface. In the adsorption process, the O_2 molecule will dissociate and occupy two so-called active sites, while the CO adsorbs intact and occupy a single site. Next, the adsorbed and dissociated CO and O react with each other to form CO_2, which desorbs from the surface.

The main function of the catalyst is that it provides an alternative reaction path, including adsorption on and desorption from the surface. This means that the reaction process becomes more complex, but the involved reaction barriers are lower, and as explained above, this significantly increases the rate constant and hence the reaction rate. Returning to the Maxwell-Boltzmann distribution in Figure 4.1, this can be illustrated by the higher activation energy, $E_{a,1}$, corresponding to the non-catalyzed reaction, while the lower activation energy, $E_{a,2}$ corresponds to the catalyzed reaction.

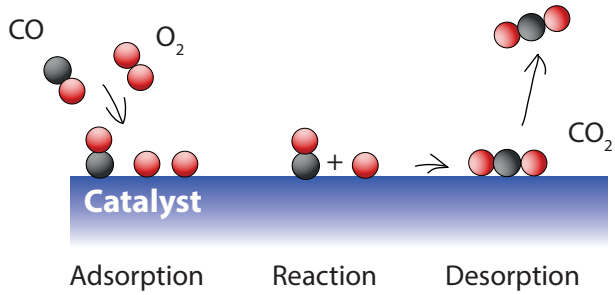

Figure 4.3: Model of the heterogeneous catalytic oxidation of CO. O_2 and CO can adsorb on the catalyst surface and O_2 molecule can disassociate into two O atoms. CO can react with one O atom, form CO_2 and desorb from the surface.

As the catalytic reaction, however, is divided into several steps, each of these part reactions have its own rate law and rate constant. Often, there is one of these steps that has a higher activation energy than the other. With the exponential dependence for the rate constant on the activation energy, this means that all the other steps have a significantly higher rate, and the rate of the total reaction is determined by this single step. This is called the rate limiting step.

For the catalysed reaction, CO and O_2 adsorb on the surface, forms CO_2, which leaves the surface. The reaction is divided into the following steps.

$$O_2 + ** \rightarrow 2O* \tag{4.7}$$
$$CO + * \rightarrow CO* \tag{4.8}$$
$$O* + CO* \rightarrow CO_2 * + * \tag{4.9}$$
$$CO_2* \rightarrow CO_2 + * \tag{4.10}$$

where, O_2 and CO are two reactant molecules, * is an active site on the catalytic surface, where the reactants can adsorb. O* and CO* are adsorbed O and CO and CO_2 is the final product. Among these, the adsorption and desorption steps have very low activation energies, and the rate limiting step is the formation of CO_2.

One must not forget, however, that the rate constant is not the only thing controlling the reaction rate. If there are no reactants available, the reaction cannot proceed, as described by the concentration terms in the rate law, Equation 4.2. In the catalyzed reaction, this does not only include the actual reactant molecules, but also available active sites, that act as reactants for the adsorption steps. This becomes crucial in the case of CO oxidation over Rh at low temperatures, where CO tends to cover the surface and significantly limit the available

adsorption sites for O_2. Hence, although the rate constant is very high, the rate of O_2 adsorption, and the whole reaction, is very low. In order for the reaction to take place, CO first has to desorb from the surface. On Rh(111), this process has an activation energy of about 1.1 eV [58] and hence becomes the rate determining step.

Finally, while testing how good a catalyst is, the reaction rate is often normalized against the number of active sites on the surface. The **catalytic activity** is then expressed as the so-called turnover frequency, that is the number of produced product molecules per active site per second.

4.3 Catalytic Reaction Mechanisms

In order to properly understand a catalytic reaction, it is important to know how the reaction proceeds, that is the reaction mechanism. There are three reaction mechanisms that are relevant for this thesis. Below, catalytic CO oxidation will be used to illustrate them.

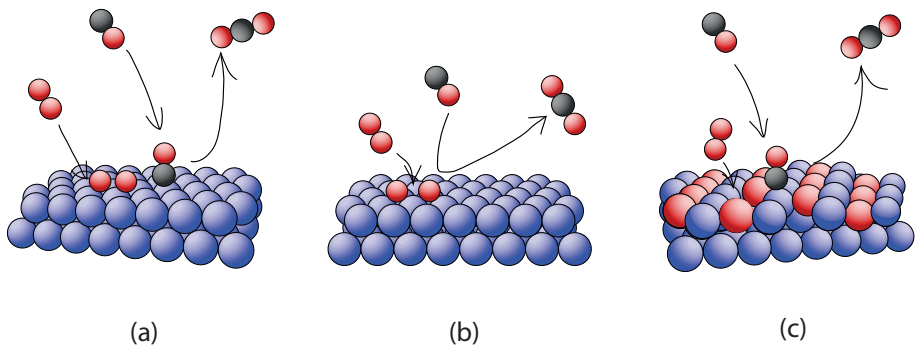

Figure 4.4: Reaction mechanisms relevant for this thesis, illustrated by CO oxidation. (a) Langmuir-Hinshelwood mechanism, (b) Eley-Rideal mechanisms, (c) Mars-Van Krevelen mechanism.

The **Langmuir-Hinshelwood mechanisms**, which was used in the example above, is illustrated in Figure 4.4(a). It was suggested by Irving Langmuir in 1921 and developed further by Cyril Hinshelwood in 1926 [59]. The mechanisms illustrates that, firstly, the two reactant molecules O_2 and CO adsorb on the surface and O_2 dissociates. Secondly, the chemical reaction takes place on the catalytic surface, resulting in the formation of a new molecule, CO_2 as the product, and eventually the product desorbs from the surface [60]. As described above, this mechanism involves the following reaction steps.

$$O_2 + ** \rightarrow 2O* \tag{4.11}$$
$$CO + * \rightarrow CO* \tag{4.12}$$
$$O* + CO* \rightarrow CO_2 * + * \tag{4.13}$$
$$CO_2* \rightarrow CO_2 + * \tag{4.14}$$

Some of the catalytic reactions observed in the present thesis follow the Langmuir-Hinshelwood mechanisms. In **Paper II**, oxygen adsorb dissociatively on a Rh surface and reacts with two adsorbed CO molecules, forming two CO_2 molecules which subsequently desorb from the surface.

The second mechanism is called the **Eley-Rideal mechanisms** and is shown in Figure 4.4(b). D. D. Eley and E. K. Rideal proposed this mechanism in 1938. They suggested that one of the reactant molecules adsorb onto the surface while the second reactant will react with adsorbed molecule without adsorbing on the surface. For CO oxidation, this would correspond to the following two steps.

$$O_2 + ** \rightarrow 2O* \tag{4.15}$$
$$O* + CO \rightarrow CO_2 + * \tag{4.16}$$

The third reaction mechanism is called the **Mars-Van-Krevelen mechanisms** and is shown in Figure 4.4(c) and was described by Mars-Van-Krevelen in 1954. The difference from the other two mechanisms is that one of the reactant is a part of the catalytic surface, such as oxygen atoms in a surface oxide. The second reactant adsorbs onto the catalytic surface and reacts with an atom from the surface structure, which is later on replaced by adsorption of the first reactant from the gas phase. In the case of CO oxidation, O_2 adsorbs and oxidizes the surface, CO then adsorbs on the surface and reacts with the oxygen in the oxide to form CO_2 [48]. In **Paper III**, a 1D oxide on a faceted Rh(553) surface provides the oxygen for the catalytic oxidation of CO following the Mars-Van-Krevelen mechanisms:

$$O + M \rightarrow MO \tag{4.17}$$
$$CO + * \rightarrow CO* \tag{4.18}$$
$$MO + CO* \rightarrow CO_2 + * + M \tag{4.19}$$

Chapter 5

Experimental techniques

A fundamental understanding of the relation between catalytic activity and surface structure often needs several techniques. In this work, I have used X-ray Photoelectron Spectroscopy (XPS), Surface X-Ray Diffraction (SXRD) and low-energy electron diffraction (LEED) in order to gain comprehensive information about the interaction between reactants and the surface of a model catalyst [61–63]. XPS can determine the binding energy of electrons from atoms in the surface region of the sample, which is directly related to the elemental composition and chemical state of the sample surface. In addition, thorough analysis may provide information on film thicknesses and depth profiles [64–66]. Diffraction techniques, on the other hand, determine the periodicity of the sample, and indirectly the atomic positions. Furthermore, surface diffraction provides information on the surface orientation and surface roughness [67]. In addition, the experimental results are complemented with Density Functional Theory (DFT) calculations, performed by collaborators.

The principles of XPS and diffraction are described in this chapter. For diffraction the basic theory is described followed by a discussion of the differences between SXRD and LEED.

5.1 Diffraction

Diffraction is a widely used analytical technique for material characterization. It is used to identify phases and determine orientations, crystallite sizes, and crystallographic structures. Diffraction occurs when radiation is scattered by a crystalline structure, producing a pattern of constructive interference at cer-

tain angles. This diffraction pattern is uniquely related to the periodicity of the atoms in the material and can be used to determine the structure of an unknown material, or as a fingerprint of a known material [68]. Diffraction can be applied on solid crystals or powders and depending on the kind of probe used, almost all materials can be investigated. While electron diffraction does not work on insulating materials, X-ray diffraction has no limitation of electrical conductivity.

5.1.1 Introduction to diffraction

An incoming wave that interacts with an object, will be scattered in all directions. To simplify the theory, we only consider elastic scattering, that is without any energy loss during the scattering, so that the in- and outgoing waves have the same wavelength. Waves scattered by different objects will interfere with each other when they meet. When they are in phase, the interference will be **constructive** and their amplitudes will be added into a larger resulting wave. When the waves are out of phase, the interference will be **destructive** and the two waves cancel each other. This is illustrated in Fig 5.1 A.

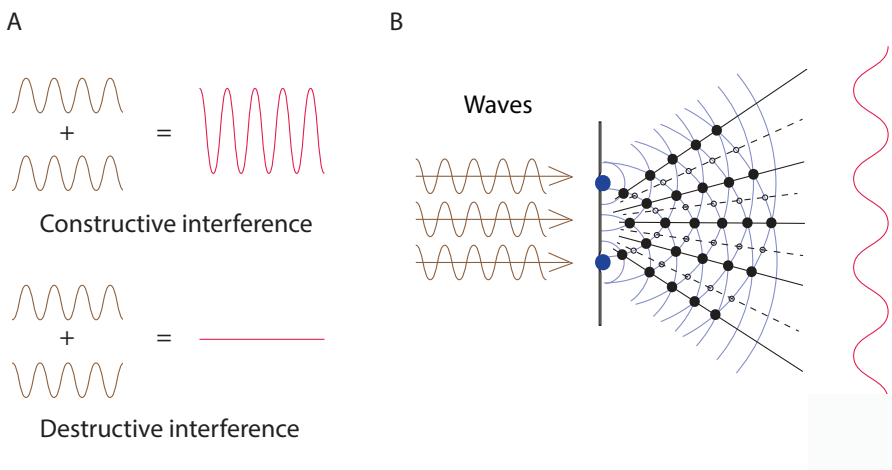

Figure 5.1: A. Constructive and destructive interference. B. Scattering from two objects. In the directions where the scattered wave are in-phase, there will be an intensity maximum, as shown by the red intensity curve.

A crystal has a structure consisting of an array of periodically separated atoms,

and diffraction provide information about the atomic arrangement within the crystal. We assume that the scattering is homogeneous, such that the interference pattern from a 1D array of atoms corresponds to the interference pattern from a multiple slit system. The intensity distribution from such a system is given by

$$I \propto \left(\frac{\sin N\pi x}{\sin \pi x} \right)^2 \tag{5.1}$$

Here, I is the intensity, N is the number of slits or atoms and $x = PD/\lambda$ is the path difference between two adjacent scattered rays relative to the wavelength. [68–71].

Figure 5.2 shows the intensity distribution, according to Equation 5.1[72], for systems of 1, 2, 4, 8, 16 and an infinite number of slits or atoms. The main peaks show where the constructive interference is maximized. These directions do not depend on the number of atoms involved in the scattering. Instead, the number of atoms affects the sharpness of the interference pattern, such that the more atoms that are involved, the sharper and more intense are the peaks. In addition, for more than two atoms, there are also secondary maxima appearing in the directions where the waves from some atoms are in phase, while others are out of phase. These secondary maxima become weaker and weaker as the number of atoms increases, and for an infinite number of atoms, all the intensity is concentrated in the main diffraction peaks, which are infinitely sharp.

5.1.2 General diffraction theory

For a more thorough derivation of the diffraction theory, Figure 5.3 shows a wave coming in from the left and and two rays being scattered by two different atoms separated by the vector $\mathbf{R}$. The traveled path difference (PD) between the two rays, is the sum of the projections of $\mathbf{R}$ on each direction of incoming and outgoing rays. According to Figure 5.3, we can describe the path difference as

$$PD = S + S' = R\cos\theta + R\cos\theta' \tag{5.2}$$

where we $R = |\mathbf{R}|$. In order to have a full constructive interference between these two rays, the path difference should be an integer number of wavelengths

$$PD = n\lambda \tag{5.3}$$

Let us now describe the incoming and outgoing waves with their wave vectors, $\mathbf{k}$ and $\mathbf{k}'$, respectively with

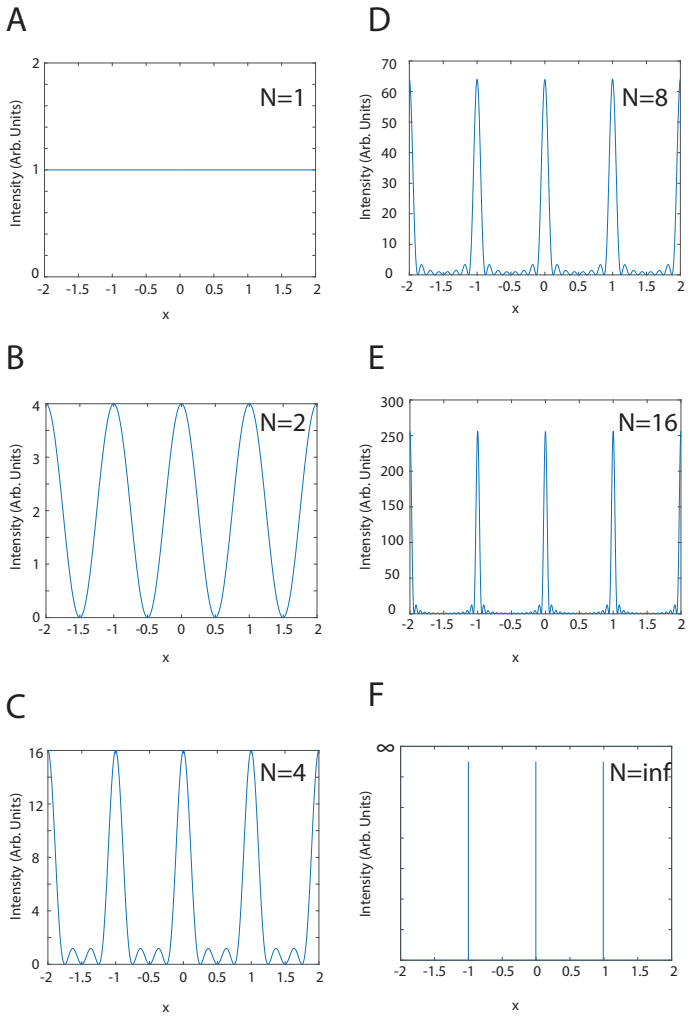

Figure 5.2: Simulation of interference in slits. A-F represent 1, 2, 4, 8, 16 and an infinite number of slits. The more slits the sharper interference peaks.

$$k = |\mathbf{k}| = |\mathbf{k}'| = \frac{2\pi}{\lambda} \tag{5.4}$$

We then get

$$\mathbf{R} \cdot \mathbf{k} = Rk\cos(180^\circ - \theta) = -Rk\cos\theta \tag{5.5}$$

and

$$\mathbf{R} \cdot \mathbf{k}' = Rk\cos\theta' \tag{5.6}$$

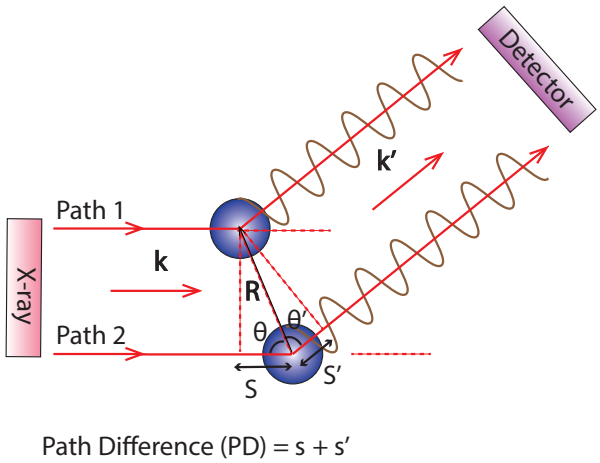

Figure 5.3: A wave is scattered by two atoms and a detector looking for intensity in a certain direction. This, in turn happens when the path difference (PD) is an integer times the wavelength, $PD = s + s' = n\lambda$.

By defining $\mathbf{\Delta K}$ as the change in wave vector, $\mathbf{\Delta K} = \mathbf{k}' - \mathbf{k}$, we get constructive interference if

$$\frac{\mathbf{R} \cdot \mathbf{\Delta K}}{k} = \frac{\mathbf{R} \cdot \mathbf{k}}{-k} + \frac{\mathbf{R} \cdot \mathbf{k}'}{k} = S + S' = PD = n\lambda = n\frac{2\pi}{k} \tag{5.7}$$

and

$$\mathbf{R} \cdot \mathbf{\Delta K} = 2\pi n \tag{5.8}$$

5.1.2.1 Real and reciprocal lattice

The atoms in a crystalline material are arranged in a periodic lattice described by the basis vectors $\mathbf{a_1}$, $\mathbf{a_2}$ and $\mathbf{a_3}$. A general lattice vector $\mathbf{R}$, connecting two lattice points, is then described by

$$\mathbf{R} = m_1\mathbf{a_1} + m_2\mathbf{a_2} + m_3\mathbf{a_3} \tag{5.9}$$

where m_i are integers. Intense diffraction peaks are found if the condition in equation 5.8 is fulfilled for all atoms in the crystal simultaneously, that is for all possible lattice vectors, $\mathbf{R}$.

The diffraction pattern corresponds to the reciprocal lattice, which is the Fourier transform of the atomic lattice [73]. A general reciprocal lattice vector is described by

$$\mathbf{G} = q_1\mathbf{b_1} + q_2\mathbf{b_2} + q_3\mathbf{b_3} \tag{5.10}$$

where q_i are integers and the relation between the real and reciprocal basis vectors can be described by

$$\mathbf{b}_1 = 2\pi\frac{\mathbf{a}_2 \times \mathbf{a}_3}{\mathbf{a}_1 \cdot (\mathbf{a}_2 \times \mathbf{a}_3)}, \mathbf{b}_2 = 2\pi\frac{\mathbf{a}_3 \times \mathbf{a}_1}{\mathbf{a}_2 \cdot (\mathbf{a}_3 \times \mathbf{a}_1)}, \mathbf{b}_3 = 2\pi\frac{\mathbf{a}_1 \times \mathbf{a}_2}{\mathbf{a}_3 \cdot (\mathbf{a}_1 \times \mathbf{a}_2)} \tag{5.11}$$

This means that $\mathbf{b}_1$ is perpendicular to $\mathbf{a}_2$ and $\mathbf{a}_3$, and similar for $\mathbf{b}_2$ and $\mathbf{b}_3$, and that the length relation is $b_1 : b_2 : b_3 = 1/a_1 : 1/a_2 : 1/a_3$.

For simplicity, the illustration of a 2D lattice for (A) real space and (B) reciprocal space is shown in Figure 5.4, where $\mathbf{b}_1 \perp \mathbf{a}_2$, $\mathbf{b}_2 \perp \mathbf{a}_1$ and $b_1 : b_2 = 1/a_1 : 1/a_2 = a_2 : a_1$. As a special case for 2D lattices, the result is that the shape of the reciprocal lattice is similar to that of the real lattice, but rotated 90°.

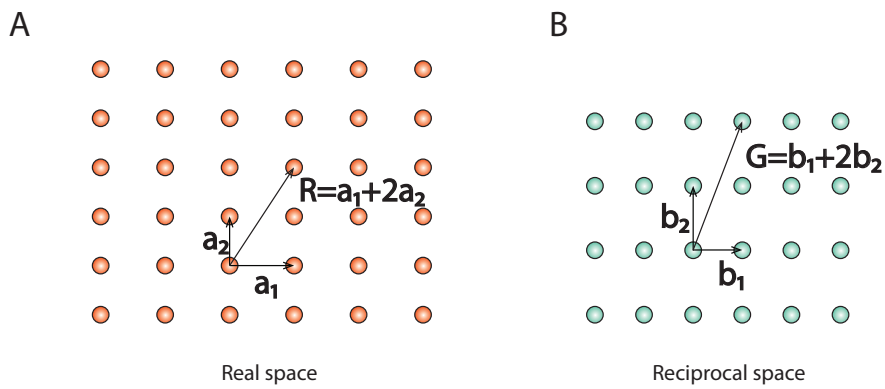

Figure 5.4: A 2D rectangular real (a) and corresponding reciprocal (b) lattice. For 2D lattices, the shape of the real and reciprocal lattices are similar, but rotated 90°.

5.1.2.2 The Laue condition

Since the reciprocal lattice vector, $\mathbf{G}$, and the wave vectors, $\mathbf{k}$, $\mathbf{k}'$ and $\mathbf{\Delta K}$, have the same dimension of inverse length, they can be described by the same basis. Especially

$$\mathbf{\Delta K} = h\mathbf{b}_1 + k\mathbf{b}_2 + l\mathbf{b}_3 \tag{5.12}$$

where h, k and l does not have to be integers.

The diffraction condition (equation 5.8) can then be described as

$$\begin{aligned} 2\pi n = \mathbf{R} \cdot \mathbf{\Delta K} &= m_1 h\mathbf{a}_1 \cdot \mathbf{b}_1 + m_2 k\mathbf{a}_2 \cdot \mathbf{b}_2 + m_3 l\mathbf{a}_3 \cdot \mathbf{b}_3 \\ &= (m_1 h + m_2 k + m_3 l)2\pi \end{aligned} \tag{5.13}$$

Therefore,

$$(m_1 h + m_2 k + m_3 l) = n \tag{5.14}$$

In order for this to be fulfilled for any $\mathbf{R}$, that is for any combination of m_1, m_2 and m_3, h, k and l need to be integer numbers. This means that a diffraction peak appear in the directions where $\mathbf{\Delta K}$ is a reciprocal lattice vector, or

$$\mathbf{\Delta K} = \mathbf{G} \tag{5.15}$$

which is called the Laue condition.

5.1.2.3 The Ewald sphere

Figure 5.5 shows, for a 2D lattice, how the diffraction corresponding to reciprocal lattice point $(-2, 3)$ is measured. With a certain orientation between $\mathbf{k}$ and the reciprocal lattice, that is between the incoming beam and the crystal, $\mathbf{\Delta K}$ can reach any point on the circle, depending on the choice of $\mathbf{k}'$, that is the position of the detector. In three dimensions, this circle becomes a sphere, the so-called Ewald sphere.

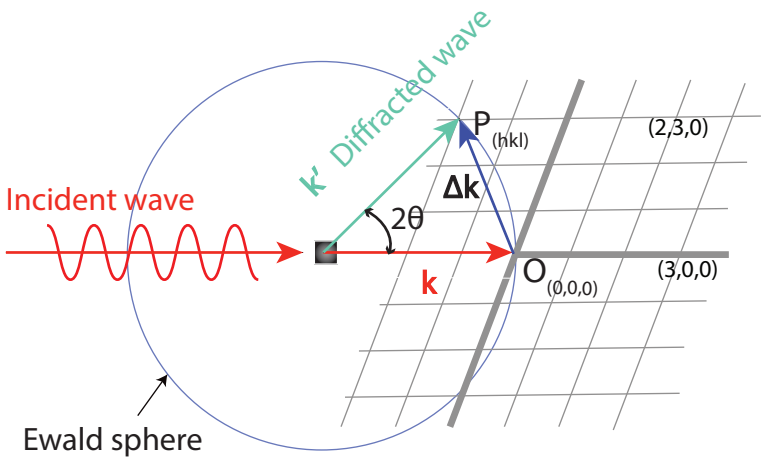

Figure 5.5: 2D representation of the Ewald sphere. The incoming wave vector, $\mathbf{k}$ points at the $(0, 0)$ point. The outgoing wave vector, $\mathbf{k}'$, and the change in wave vector, $\Delta\mathbf{K}$ points at the probed point in reciprocal space. Depending on the position of the detector, all the points along the Ewald sphere can be probed.

In order to probe other parts of reciprocal space, there are two possibilities. In X-ray diffraction, the sample, and hence the reciprocal lattice, is usually rotated such that the desired point coincides with the Ewald sphere, and the detector is moved to the corresponding direction, see figure 5.7. In LEED, on the other

hand, one instead changes the energy of the electron beam, and hence the size of the Ewald sphere.

In **Paper IV**, **Paper V** and **Paper VI**, we pioneered the use of a large 2D detector, which covered a large range of diffraction angles without moving. In this case, the 3D reciprocal space can be probed by only rotating the sample, which speeds up the measurements by several orders of magnitude.

5.1.3 Surface Diffraction

In most diffraction studies, the number of atoms contributing to the diffraction pattern is large, such that the diffraction spots, according to Figure 5.2, becomes very sharp. For a 3D sample, the result is a sharp 3D diffraction pattern, where the maxima are called Bragg reflections. The position and intensity of these reflections will give the bulk structure. But in this thesis the aim is the surface structure.

By limiting the number of atoms, the peaks becomes broader, as illustrated in Figure 5.2. In surface diffraction, we limit the number of layers contributing to the diffraction, while parallel to the surface plane, the number of contributing atoms is still very large. The result is that perpendicular to the surface, the diffraction peaks get broader, while parallel to the surface, they are sharp. Hence, the Bragg reflections turn into so-called Crystal Truncation Rods (CTRs), if diffraction is from the surface of a bulk crystal, or superstructure rods, if originating from another structure on top of the substrate surface, and by studying this rods rather than the Bragg reflections, information on the surface structure can be achieved.

The intensity variation along these CTRs or superstructure rods varies depending on the number of layers contributing. In the extreme case with only a single layer, which would for instance be a qualitative approximation of the surface oxides on Rh or Pd, this would result in rods without any intensity variations, in analogy with Figure 5.2 A. For larger number of layers, the Bragg reflections along the CTRs become stronger and stronger. This is illustrated in Figure 5.6, schematically showing how a single layer results in solid rods without any intensity variations (A), an intermediate number of layers result in Bragg reflections and CTRs (B), and a large number of layers results in sharp Bragg reflections only. In addition, any relaxation of the surface layers also alters the shape of the CTRs. Hence, by measuring the intensity along the CTRs, the surface structure can be investigated quantitatively.

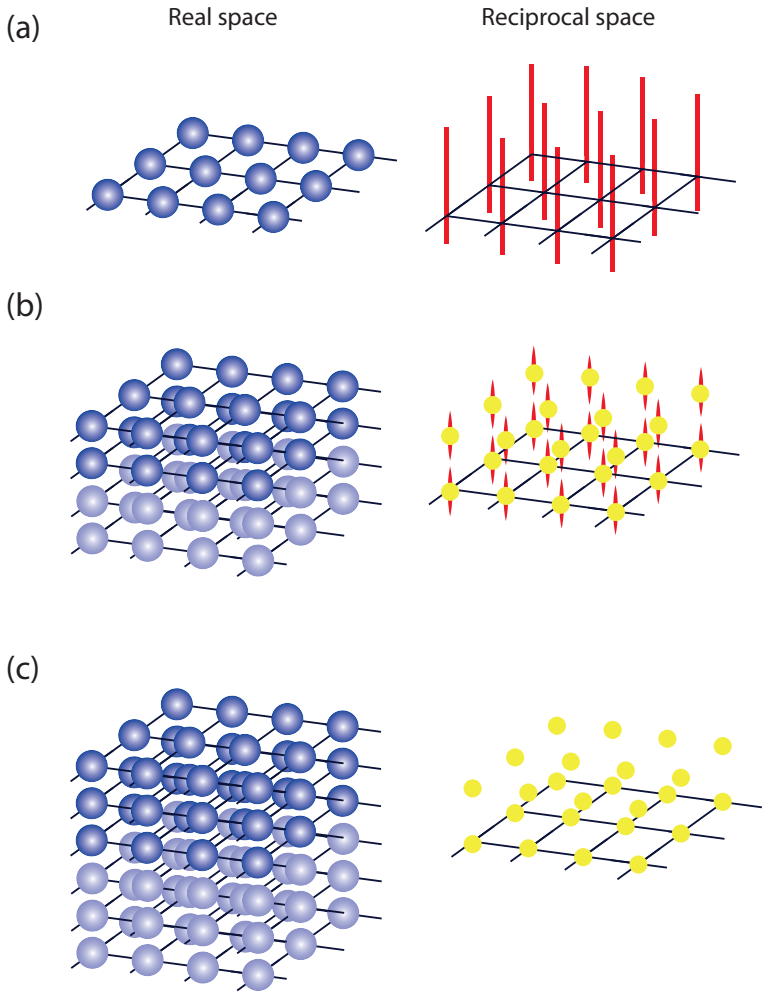

Figure 5.6: Illustration of the how the reciprocal lattice depends on the number of layers contributing to the diffraction. (a) A single layer give constant CTRs, (b) A few layers give CTRs connecting Bragg reflections, and (c) a large number of layers give Bragg reflections, only.

5.1.3.1 Surface X-Ray Diffraction

The main diffraction method used in this thesis is Surface X-Ray Diffraction (SXRD). Due to the low interaction between X-rays and matter, X-ray diffraction is usually used for bulk studies, but by letting the x-rays hit the surface under grazing incidence, preferably below the critical angle for total reflection, the number of contributing layers are limited and the surface signal becomes available.

Figure 5.7A illustrate how this measurement is performed. The X-ray beam

comes in from the left and is scattered by the crystal. Concentrating on the $(-1, 1, l)$ CTR, it intersects the Ewald sphere at the green spot. By placing the detector in the corresponding $\mathbf{k}'$ direction, the diffracted intensity of the CTR at this l is measured. In Figure 5.7B, the sample and the reciprocal lattice is rotated slightly, such that the $(-1, 1, l)$ CTR intersects the Ewald sphere at a lower l value. Thus, by rotating the sample and moving the detector, the intensity along the CTR, or any other line in reciprocal space can be measured. To map out the reciprocal space using this approach is, however, very time consuming. In **Paper IV**, **Paper V** and **Paper VI**, we pioneered the use of a large 2D detector [74], which covered a large range of diffraction angles without moving. In this case, the 3D reciprocal space can be probed by only rotating the sample, which speeds up the measurements by several orders of magnitude.

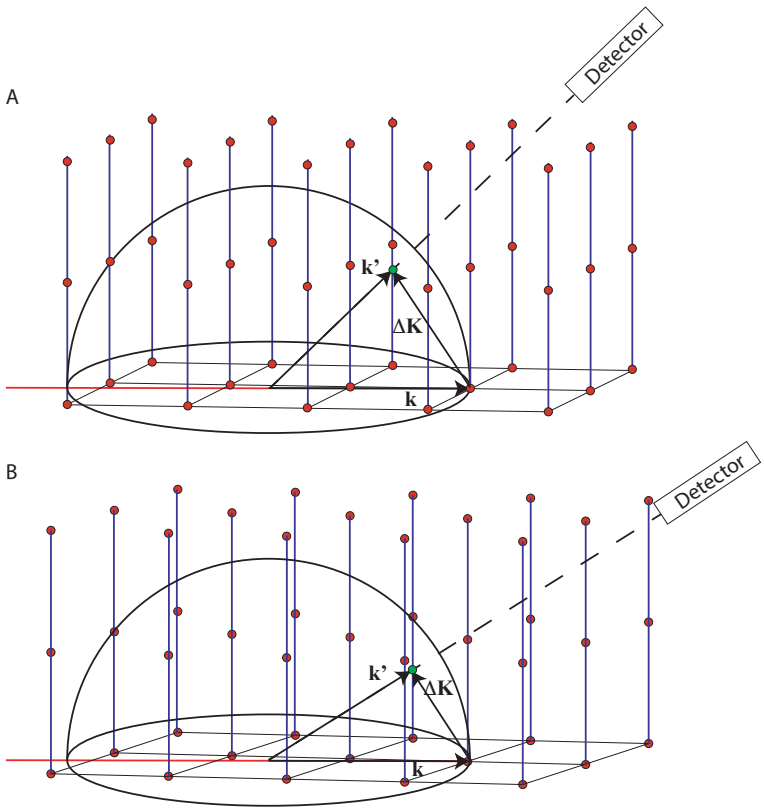

Figure 5.7: Illustration of the SXRD measurements. Concentrating on the $(-1, 1)$ rod, this intersects the Ewald sphere at the green dot, and this point is probed by placing the detector in the corresponding $\mathbf{k}'$ direction. Between panel A and B, the sample has been rotated slightly, such the the intersection point is lower and the detector needs to be moved slightly. Hence, by rotating the sample and following with the detector, the intensity along the CTRs can be probed.

As an example, Figure 5.8 shows measurements of Rh(553) from **Paper I**, where

a plane in reciprocal space close to the Bragg reflection at $(h, k, l) = (0, -4, 7)$ is mapped out at under different conditions. In panel A, the clean surface is probed, and there is a strong vertical CTR at $k = -4$ revealing the presence of the (553) surface. There is also a CTR at $k = -5$ originating from the Bragg reflection at $(h, k, l) = (0, -5, -6)$. In addition, there is a rod perpendicular to the (111) planes, diagonally between these two Bragg reflections. This is because of the (111) facets that are always present on the (553) surface.

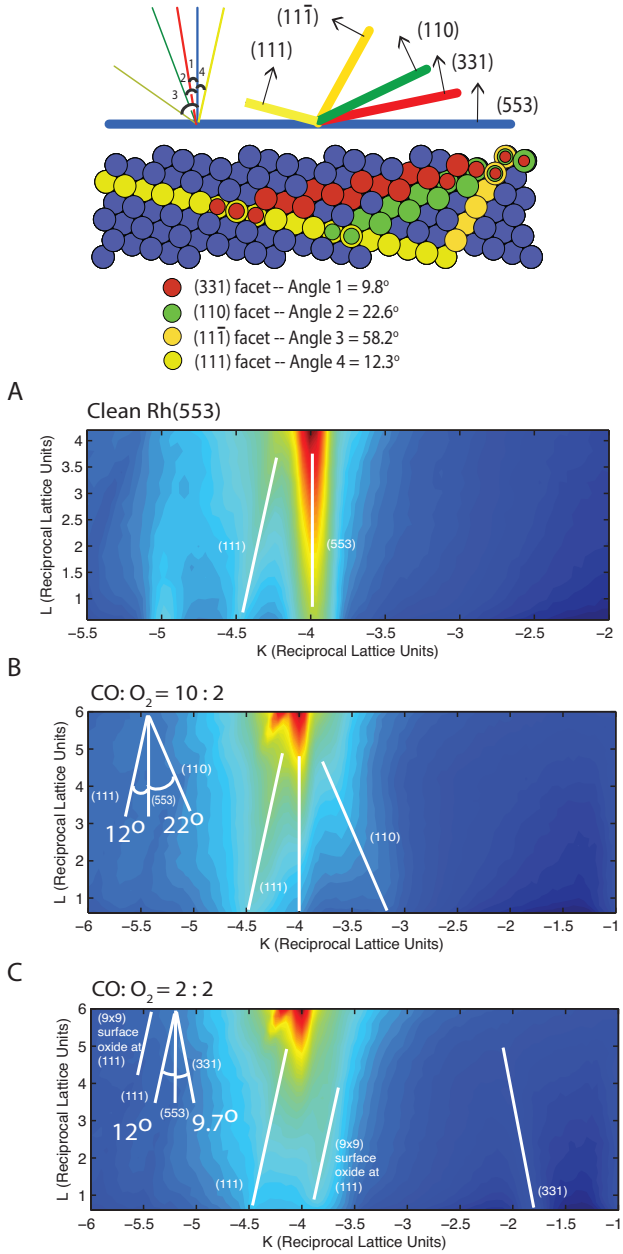

Figure 5.8: Surface X-ray Diffraction plots from Rh(553) in a CO and O_2 gas mixture during reaction. The fact that CTRs are perpendicular to the surface is used to follow the faceting of the surface. The top panel illustrates the model of the Rh(553) surface with different gas-induced facets, as discussed in Chapter 3.2.3. The bottom group of plots: Surface X-ray Diffraction plots with crystal truncation rods in different directions. (A) For the clean surface, the main CTRs are perpendicular to the (553) surface. In addition, there is a weak CTR in the [111] direction, revealing the presence of (111) facets. (B) Under CO rich condition, an additional (110) CTR is found revealing the faceting into (110) facets. (C) In an O_2 rich gas mixture, the surface is oxidized and form (9×9) surface oxide, which is formed on (111) terrace, therefore the rod leans the same direction as (111). There are also (331) CTRs revealing the presence of (331) facets with 1D oxide.

Figure 5.8 B shows the measurements during CO oxidation in an excess of CO, where the steps, as discussed in Chapter 2, are pushed closer together into (110) facets, coexisting with larger (111) terraces. This is revealed in the SXRD measurement by an increase of the (111) CTR as well as the appearance of a CTR perpendicular to the (110) planes, on the expense of the intensity of the vertical (553) rods. In oxygen excess (Figure 5.8 C), the CTR perpendicular to the (331) planes reveals the growth of the corresponding facets, where the steps are covered by the 1D oxide. In addition, a new (111) oriented rod, which does not pass through the Bragg reflections, appears due to the formation of the surface oxide on the (111) terraces. A similar study is presented in **Paper IV** for the Pd(553) surface.

5.1.3.2 Low Energy Electron Diffraction

The most common diffraction method for surface science studies is Low Energy Electron Diffraction (LEED), which makes use of the strong interaction between the charged electrons and matter to limit the number of layers contributing to the diffraction and enable the measurements of the CTRs. Figure 5.9 shows the so-called universal curve of inelastic mean free path, with experimental data of the average distance electrons will travel in metals before they lose energy. The mean free path depends on the energy of the electrons, but not significantly on the material. In a range of about 15-500 eV, the inelastic mean free path is below 1 nm. This means that the electrons that reach the detector without energy loss will predominantly originate from the surface of the sample, and methods, such as XPS and LEED, that are based on low-energy electrons will be intrinsically surface sensitive and are standard in surface science. It is important to note that, although most of the signal will originate from the surface, the scattering process is random and some electrons will travel very far in the material before they are scattered. Hence, the measurements will always include contributions from deeper layers, although the corresponding signal will be rather weak.

LEED is based on the fact that electrons can be described as waves with the wavelength depending on the kinetic energy according to the modified de Broglie equation [55, 78]

$$\lambda(\text{Å}) = \sqrt{\frac{150.6}{E(\text{eV})}} \tag{5.16}$$

This shows that electron energies between 15 and 500 eV, where the surface sensitivity is maximized, correspond to wavelengths of about 0.5-3 Å, well suited for diffraction studies [20, 79].

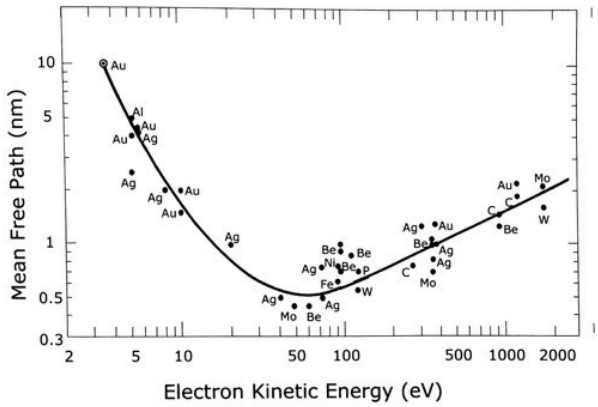

Figure 5.9: The universal curve for the electron mean free path. Optimum surface sensitivity is obtained with electrons in the 15-500 eV range. [7, 75–77]

A sketch of the LEED experiment is shown in the Figure 5.10 a. An electron gun generates an electron beam that is directed onto the sample surface with normal incidence and the backscattered electrons are collected on a fluorescent screen [9, 55]. In order for the beam paths not to be effected by any external electric fields or charging of the sample, the sample and the grid G_3 is grounded. The diffraction theory described above is based on the assumption that the electrons are scatted elastically. G_2 serve as a cut-off filter and is set to a negative potential matching the accelerating voltage in the electron gun, such that any electrons that have lost energy during the scattering process are stopped from reaching the fluorescent screen. In order for the screen to light up when hit by the electrons, the kinetic energy of the electrons have to be very high. Therefore, the screen is at a positive potential of about 6 keV. G_1 is there in order for the strong field from the screen not to affect the function of the other grids.

The LEED process is illustrated in Figure 5.10 (b). The incoming wave vector $\mathbf{k}$ hits the reciprocal surface lattice under normal incidence and is scattered to $\mathbf{k}'$. The corresponding $\Delta\mathbf{K}$ lie on the Ewald sphere, as described above, and in the $\mathbf{k}'$ directions corresponding to $\Delta\mathbf{K}$ vectors reaching a CTR, there will be a diffraction maximum. Due to the high surface sensitivity, in a qualitative study of the surface peridocity, it does not matter where the Ewald sphere intersects the CTRs. This means that the measurement is independent of the component of $\Delta\mathbf{K}$ that is perpendicular to the surface and we only need to consider the parallel component, $\Delta\mathbf{K}_{\parallel}$, which due to the normal incidence is also equal to $\mathbf{k}'_{\parallel}$. If $\mathbf{k}'_{\parallel}$ reaches from one reciprocal lattice point another, we will see the corresponding diffraction spot from the screen. Therefore, In order to have constructive interference between the diffract, the changes of parallel

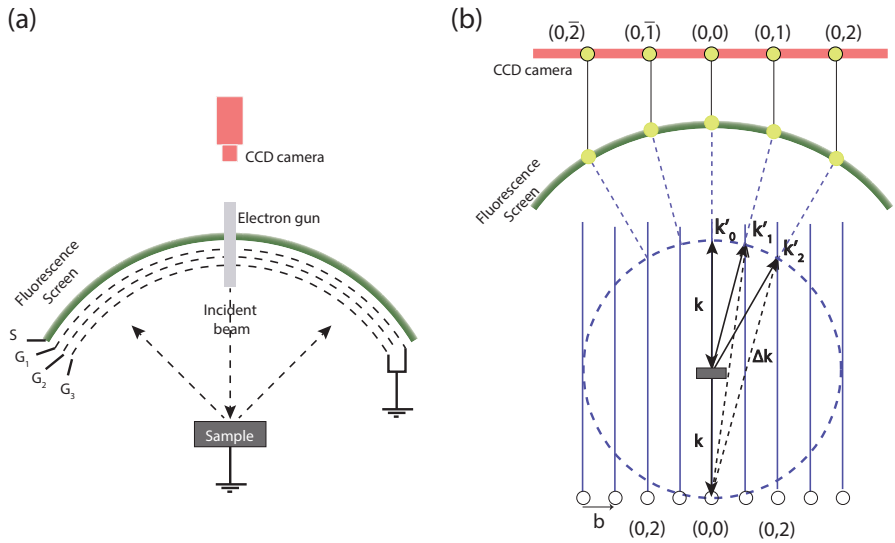

Figure 5.10: Low energy electron diffraction (LEED). (a) The fluorescent screen shows a picture of the reciprocal surface lattice. The straight dash lines indicate the direction of electron path for both incident beam and back scattered electrons. The sample is placed in the center of cruvature for the screen. G_1, G_2 and G_3 are grids making sure that the scattering is elastic and that the space around the sample is free from electric fields.

momentum needs equal a reciprocal surface lattice vector:

$$\Delta \mathbf{K}_{\parallel} = \mathbf{G}_{\mathrm{s}} \tag{5.17}$$

If the diffraction pattern on the screen is viewed from the top, a scaled image of the reciprocal surface lattice is seen directly, without any scanning of the sample or detector. Hence, both the LEED experiment and the involved equipment is much simpler than for SXRD, and most surface science laboratories include a LEED setup in order to check the periodicity of the surface. The downside of LEED is that the electrons also interact strongly with gases and, in contrast to SXRD, LEED does not work under realistic conditions for catalysis.

In spite of the high surface sensitivity, there are still intensity variations along the CTRs. While, in SXRD, the sample is rotated in order for the Ewald sphere to intersect the CTRs at different l values, the orientation between the sample and the beam is usually fixed in a LEED setup. Instead, the intersection point between the CTRs and the Ewald sphere may be changed by varying the kinetic energy of the electrons and hence the radius of the Ewald sphere. This is often used in order to maximize the intensity of the LEED pattern, but also for quantitative measurements of the surface structure [80].

5.2 X-ray Photoelectron Spectroscopy

X-ray Photoelectron Spectroscopy (XPS) is a widely used technique for providing information about the chemical composition of surfaces, the oxidation state of the material and can also be used to distinguish different phases [20, 81]. XPS is based on the photoelectric effect, that is when a photon is absorbed by an atom and its energy is used to emit an electron, which was explained by Albert Einstein in 1905 [82]. In XPS this effect is used to determine the binding energy of the electrons in a material, thus providing a unique fingerprint of the elements in the material, but also information on their chemical states. The method was developed in the mid 1960's by Kai Siegbahn and his research group at Uppsala University, Sweden [83].

5.2.1 XPS principle

The principle of X-ray photoelectron spectroscopy is illustrated in Figure 5.11. When a sample surface is irradiated by monochromatic X-rays of high enough energy, a photoemission process takes place and a so-called photoelectron is emitted from the sample. By analyzing the kinetic energy of the photoelectron, its binding energy, E_b, is found through

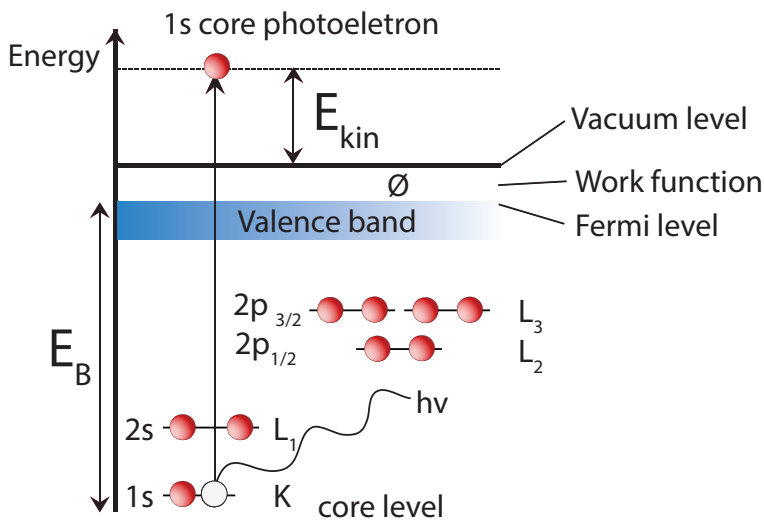

Figure 5.11: A diagram of the principle of X-ray photoelectron spectrocopy (XPS). The X-rays interact with a solid surface, resulting in the emission of a photoelectron. The binding energy is calculated from the difference between the photon energy and the kinetic energy plus the work function, as shown in equation 5.18.

$$E_b = hv - E_k - \phi \tag{5.18}$$

where h_ν is the photon energy and E_k is the kinetic energy. Here the binding energy is defined as the energy relative to the Fermi level, while the work function, ϕ, is the energy needed to lift an electron from the Fermi level to the vacuum level. The number of electrons emitted as a function of their binding energy then provide a photoelectron spectrum. As the electron levels are unique for each element, this first of all provides information on the elements that are present in the surface.

5.2.2 Chemical shifts

While the electron binding energies in an atom are mainly determined by what kind of atom it is, they are also affected by the atoms environment. If the atom makes chemical bonds to other atoms, their valence electrons will mix, and the corresponding part of the XPS spectrum will change drastically. Core electrons, on the other hand, do not take such a direct part in the bonds with other atoms, and are still possible to identify. Their binding energies do, however, still change slightly. These chemical shifts are used to investigate the chemical state of the atoms in a sample.

Most commonly, the chemical shifts are used to determine the oxidation state, that is the number of electrons each metal atom has donated, for instance, to oxygen atoms in an oxide structure. For each electron that is removed, the remaining electrons are more strongly bound and the binding energy, correspondingly increases. Also more subtle changes of the electronic structure are, however, possible to detect, especially with modern XPS at synchrotron radiation sources, where the resolution is very high. For a metal surface, it is possible to distinguish between the atoms in the bulk or on the surface of a crystal and for adsorbates it is possible to distinguish between different adsorption sites. In section 5.2.5, this is illustrated with an example of CO and O adsorption on Rh(553).

5.2.3 XPS analysis

In the XPS experiments in this thesis, the main aim is to identify different chemical environments for CO and O on Rh or Pd, and follow how the abundance of these during a catalytic reaction. The corresponding peaks, however, often

overlap with each other, and in order to retrieve information about the abundance of each species, the spectra needs to be decomposed in to individual peaks for each species. For this process, it is important to know the expected shape of each component, which is given by the convolution of Lorentzian, asymmetric and Gaussian contributions, as distried below.

The Lorentzian contribution is a result of life time broadening. When a core electron is removed, there is a finite time, Δt, until the core hole is refilled. According to Heisenberg's uncertainty principle, this gives rise an uncertainty in the energy of the excited state, and hence binding energy, which results in a broadening of the peak. The Lorentzian contribution to the line shape is described by.

$$I_L(E) = I_0 \frac{1}{\pi} \frac{\frac{1}{2}\Gamma_L}{(E - E_0)^2 + (\frac{1}{2}\Gamma_L)^2} \tag{5.19}$$

where, I_0 is the maximum intensity at the peak at E_0 position, E is the kinetic energy of the photoelectrons and Γ_L is the Lorentzian full width at half maximum.

A photoemission peak from a metallic sample generally appears asymmetric, with a tail towards higher binding energy. The origin of this asymmetry is that, during the photoemission process, not only the photoelectrons are excited, but also some valence electrons, resulting in the creation of electron-hole pairs within the valence band. This means that the measured kinetic energy of the photoelectron is slightly reduced, which according to Equation 5.18 results in a peak shifted towards higher binding energy. The asymmetry given by the asymmetry factor, α, is described by

$$f(E) \propto \frac{1}{(E_0 - E)^{1-\alpha}} \tag{5.20}$$

which convoluted with the Lorentzian gives the Doniach-Šunjić line shape [84] as

$$f(E) = \frac{\Gamma(1-\alpha)}{((E - E_0)^2 + \gamma^2)^{(1-\alpha)/2}} \cos(\frac{\pi\alpha}{2} + (1-\alpha)\tan^{-1}((E - E_0)/\gamma)) \tag{5.21}$$

The Gaussian contribution involves more or less random effects, such as instrumental broadening, thermal and vibrational effects. Also, the presence of peaks with chemical shifts that are too small to be distinguished can often be described by an increased Gaussian broadening. The Gaussian line shape is described by

$$I_G(E) = I_0 \exp(-\frac{In2(E_0 - E)^2}{\sigma^2/4}) \tag{5.22}$$

where σ is the Gaussian full width at half maximum [85].

The XPS spectra in this thesis were analyzed using the FitXPS2 software [86], using a convolution of Doniach-Šunijć and Gaussian lineshapes with a linear background.

5.2.4 Vibrational effect

In addition to the small vibrational excitations that are adding to the Gaussian broadening, in our measurement of the C 1s level of CO we see larger vibrational excitations that give rise to extra components. These excitations can be described by the Franck-Condon principle. Fig 5.12 shows a schematic diagram of the potential energy as a function of the distance between the two nuclei, for two electronic states of a diatomic molecule. In the electronic ground state, the nuclei have the equilibrium distance, r_e, but this changes to r'_e as a result of the electronic excitation. If the nuclei were separated by the equilibrium distance before the photoemission process, it will not be at equilibrium afterward, and the molecule will start vibrating [87].

This excitation of localized C-O stretch vibration during the photoemission process results in a split of the corresponding C 1s peaks [34].The energy of C-O stretch vibration varies depending on the adsorption sites. All the C1$_s$ spectra in this thesis are fitted with each CO peak being split into three vibrational components, with shifts as published by Smedh *et al.* [34]. For clarity, only the main peak is shown in the corresponding plots.

5.2.5 XPS of CO and O on Rh(553)

As an example of the use of XPS in this thesis, spectra from **Paper II** of O and CO adsorbed on Rh(553) are shown in Fig 5.13 A. Starting from the top, exposure of the clean Rh(553) surface to O_2 results in a single peak in the O 1s spectrum, corresponding to O atoms adsorbed in 3fh sites. As expected, there is no peak in the C 1s spectrum. The bottom spectrum instead is measured after exposing the clean surface to CO, which adsorbs in both 3fh and on-top sites, resulting in two different O 1s peaks.[1] In the C 1s spectrum, however,

[1]It is not well established whether the adsorption of CO on the steps are in 3fh or bridge sites. For simplicity, in this discussion it is assumed to be 3fh as on the terraces.

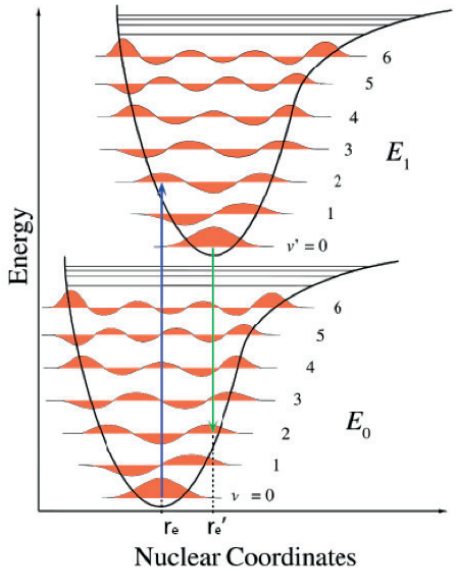

Figure 5.12: The Franck-Condon principle. The potential energy of a diatomic molecule as a function of the distance between the nuclei, for two electronic states. During the photoemission process, we have an vertical transition from the electronic ground state (E_0) to the excited state (E_1). r_e and r'_e are the corresponding equilibrium distances between nuclei, from [88].

there are now four different components as this level is more sensitive and can distinguish, not only between the kinds of adsorption sites, but also if the sites are on terraces or steps. Hence, the four components correspond to CO adsorbed in on-top sites on terraces and steps, as well as 3fh sites on terraces and steps. At this high coverage, however, the CO mainly adsorbs in the 3fh sites on the steps. Finally, the middle spectra are measured after exposing the O covered surface to CO at room temperature, such that most, but not all, of the O has been removed and replaced by CO. The O 1s spectrum reveals the presence of O in 3fh sites and CO in both 3fh and on-top sites, as might be expected. The C 1s spectrum, however, shows that the CO adsorbed on steps almost exclusively adsorb in on-top sites, in contrast to the case without O. We interpret this as showing that the remaining O is positioned in 3fh sites on the steps, hence blocking these sites for CO adsorption.

(at 285.7 eV), on top of terrace (at 286 eV), on hollow of step (at 285.3 eV) and on hollow of terrace (at 285.5 eV). Now, compare to the for O1$_s$ spectra for CO adsorption on Rh(553) with chemisorbed O, first of all, chemisorbed O peak is still there, meaning there are chemisorbed O remain on the surface. And then compare the difference between only chemisorbed CO for C1$_s$ spectra, the intensity of the peak for CO adsorb on step sites is significantly smaller than CO

on clean Rh(553). Since chemisorbed O prefer to adsorb on 3 fold hollow site for Rh surface, combining with the C1_s spectra, we interpret the remaining O is positioned on hollow of step sites. Models of the surface structures corresponding to each set of spectra are shown in Fig 5.13 B, C and D.

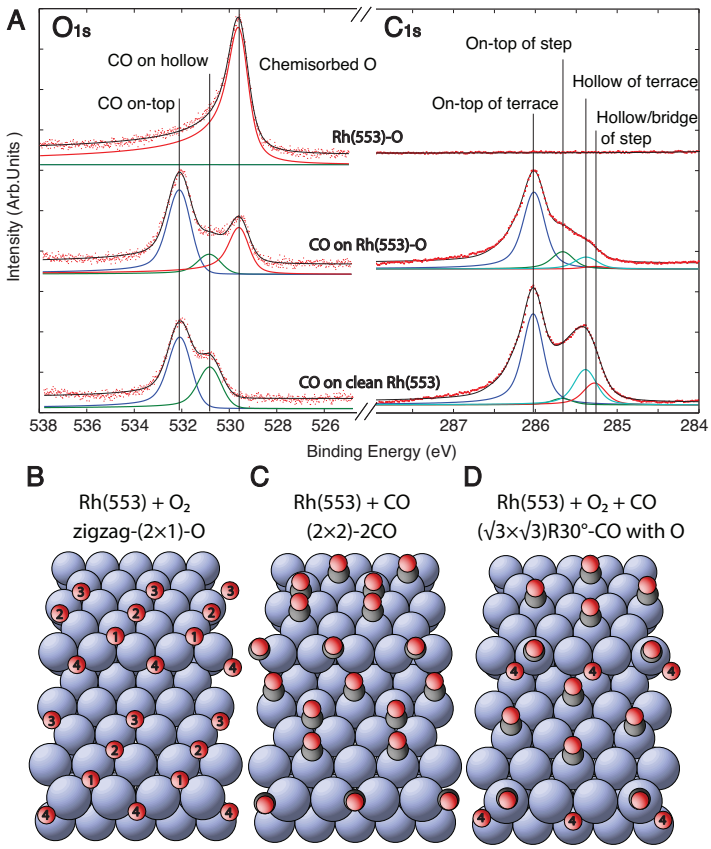

Figure 5.13: XPS measurement of CO and O adsorption on Rh(553). (A) O 1_s and C 1_s spectra corresponding to (B) chemisorbed O, (C) chemisorbed CO and (D) a coadsorption phase found after the reduction of the phase in (B) with CO. From **Paper II**

Chapter 6

Summary of Papers

This thesis includes 6 papers, with research about catalytic CO oxidation over vicinal and oxidized Rh and Pd surface. We tried to bridge the material gap using different characterization techniques to relate their surface structure to catalytic activity.

I – Faceting of Rhodium(553) in Realistic Reaction Mixtures of Carbon Monoxide and Oxygen

CO oxidation over Rh(553) was studied by Surface X-ray Diffraction and Mass Spectrometry under realistic reaction conditions. Exposing the sample to different mixtures of CO and O_2 resulted in rearrangements of the stepped surface into different facets. We found (110) facets under CO rich conditions, (553) facets close to stoichiometric conditions, (331) facets with a 1 dimensional oxide along the step edges under mildly oxidizing conditions and highly oxidizing conditions results in the formation of surface oxide over (111) and equivalent $(111\bar{1})$) facets. The facets with higher step distance, that is (331) and (101), coexist with larger (111) terraces, covered by CO or chemisorbed O.

Knowledge about this kind of rearrangements is very important since different facets have different catalytic activity. Hence, the activity of herein identified facets and oxide structures is the aim of paper II, III and V.

II – Steps and Catalytic Reactions: CO Oxidation with Preadsorbed Oxygen on Rh(553)

In this paper, we extend the study from **Paper I**, by following the reaction between CO gas and preadsorbed O on Rh(553). In order to investigate the changes in a controlled way, we performed the experiments under UHV condition. The result shown that the reduction of Rh(553) with chemisorbed O is faster than on (111) until 50% of the O has been removed, which shows that the stepped surface is more active that the flat one. The remaining 50% was, however, bound to the step edges and significantly more difficult to remove with CO, showing that it is not the step edges as such that are highly active. Instad, our DFT calculations suggest that the reaction takes place on terrace near step, and oxygen atoms from other sites need to diffuse to these active sites before the reaction can take place.

It is often believed that stepped surfaces are more active due to the low coordination of the step atoms. This study, however, shows that the reason is rather relaxation of the surface layers, which lowers the energy barrier for the CO oxidation reaction near the step. This also agrees with the results for Pd by Blomberg et al [89].

III – A Study of Reduction of Oxygen Structures on a Faceted Rh(553) Surface by CO

In Paper III, the surface with (331) and (111) facets, as identified in Paper I, was prepared in pure O_2, and reduced by exposure to CO during stepwise increasing temperature. The XPS results following the reduction show that the 1D oxide along the steps was very active and reduced first. When about 50% of this O had been removed, the remaining O was found in a chemisorbed state along the step edges and, in accordance with Paper II, relatively hard to remove since the the (331) facets are too small to expose the active near-step sites. Instead, the O from terraces was reduced next, suggesting the terraces are not too wide, such that the O can diffuse from the terraces to near-step sites, where the reaction takes place. Eventually, when the sample temperature is high enough, the chemisorbed O at the steps is also removed.

IV – Step Dynamics and Oxide Formation During CO Oxidation over a Vicinal Pd Surface

Paper IV reports an expoeriment similar to the one described in **Paper I**, following the faceting for Pd(553) during CO oxidation under realistic conditions using Surface X-ray Diffraction. Under CO rich conditions, the Pd(553) surface stays unreconstructed, covered with CO. In small excess of O_2, (332) and (331)

facets with surface oxide can be observed, while under even more O_2 rich conditions, a multilayer PdO bulk oxide with the [101] crystallographic direction is formed on (331) and (111). Hence, just like Rh(553), the Pd(553) surface undergo faceting when exposed to realistic reaction conditions. The kind of facets formed, depend on the matching with the O or CO structures formed.

From this we identify the Pd oxides based on PdO(101) as important for further studies, as done in Paper V

V – The Role of Oxides in Catalytic CO Oxidation over Rhodium and Palldium

In order to investigate which phase is more active, we started these experiments at high temperature, so that the surface gets oxidized and is highly active. We then cool down so that the reaction is slowed down. We follow the extinction (in MS) as well as the presence of the oxides (in SXRD) for Rh and Pd. The results shown that, for Rh case, the metal is more active than oxide. For Pd, the surface oxide and epitaxial bulk oxide are as least as active as the metal, but the polycrystalline thick bulk oxide is less active. The active oxides is with Coordinately Unsaturated Structure (CUS) sites.

VI – High-Energy Surface X-ray Diffraction for Fast Surface Structure Determination

A full view of the High Energy Surface X-ray Diffraction technique is described in this paper. The high energy of the X-rays results in significantly smaller scattering angles, as compared to conventional SXRD. Hence, a large 2D detector can collect a large range of diffraction angles at once. This means that more of reciprocal space can be captured at the same time, which give better time resolved measurement. Further, it is possible to map out the reciprocal space in 3D with a simple sample rotation of about 15 min. Such maps are in practice impossible to produce using conventional SXRD with small detectors. From this 3D map, it is also possible to extract quantitative data for surface structure determination, something that usually takes in the order of 10 hours to measure. For demonstrating the use of high energy diffraction, an example of surface oxide formation during reaction on Pd(100) was studied in this paper.

Chapter 7

Conclusions and Outlook

To conclude, I have studied CO oxidation over flat and stepped Rh and Pd surfaces using Surface X-Ray Diffraction (SXRD) and X-ray Photoelectron Spectroscopy (XPS), and complemented by Density Functional Theory (DFT) calculations. During CO oxidation under realistic conditions, the vicinal surfaces were found to undergo faceting, in order to match the formed oxygen or CO structures. Certain oxygen structures were then identified and studied under simplified conditions, at UHV for the stepped facets and using flat substrates for the oxide structures. The thesis highlights the fact that the atomic scale surface structure of a model catalyst is key for the understanding of a catalytic reaction.

For metallic Rh surfaces, we find that stepped surfaces has higher catalytic activity compared to low-index surface structure, in agreement with previous studies. While this difference has previously been attributed to the presence of step edges exposing atoms with low coordination, we show that the steps as such are not responsible for the high activity, but instead the active site is found on the terrace near the step, due to relaxation of the terraces. For Pd and Rh oxides, it is found that the oxides are active if there are Coordinatively UnSaturated (CUS) metal atoms exposed for CO to adsorb and react at. This is the case for thin Pd oxides, but not on 2D and 3D Rh oxides. Under mildly oxidizing conditions, however, the Rh(331) facets expose a 1D oxide along the step edges, and CO is able to adsorb just inside on the terrace. This Rh oxide structure is able to oxidize CO under significantly lower temperatures as compared to metallic Rh.

These findings can be important in the development of future oxidation cata-

lysts. The catalytic activity can be maximized by optimizing the surface step density such that the diffusion of O atoms to the active site close to the step edge is facile. Further, considering the activity of the oxides, we can understand why Pd is less sensitive to oxygen poisoning (deactivation due to exposure to too much oxygen) than Rh [90]. This effect can likely be reduced even further by producing a thin layer of Pd on an inert metallic substrate, so that the PdO will not be able to grow into thick bulk oxide which lower the catalytic activity.

The results can most likely be used, not only for CO oxidation, but also for other oxidation reaction, such as methane. Methane is the main constituent of bio- and natural gas used as fuel in cars, but also a very strong greenhouse gas. Hence it is very important to develop catalysts for removal of unburnt fuel from the exhausts of gas driven cars.

Bibliography

[1] P. H. N. Kaspar, J; Fornasiero. *Automotive catalytic converters:Current status and some perspectives.* Catal. Today 77, pp. 419–449, **2003**.

[2] G. A. Somorjai. *Introduction to Surface Chemistry and Catalysis.* Wiley, New York, **1994**.

[3] H. K. G.Ertl and J. Weitkamp. *Handbook of Heterogeneous Catalysis.* VCH, Weinheim, **1997**.

[4] A. C. A. Frennet. *Catalysis and Automotive Pollution Control.* Elsevier Science, **1987**.

[5] J. A. M. F. R. A. v. S. A. E. Van Diepen, M. Makee. *Environmental Catalysis.* Imperial College Press, London, **1999**.

[6] A. J. Medford, A. Vojvodic, J. S. Hummelshøj, J. Voss, F. Abild-Pedersen, F. Studt, T. Bligaard, A. Nilsson, and J. K. Nørskov. *From the Sabatier principle to a predictive theory of transition-metal heterogeneous catalysis.* Journal of Catalysis 328, pp. 36 – 42, **2015**. doi:https://doi.org/10.1016/j.jcat.2014.12.033. Special Issue: The Impact of Haldor Topsøe on Catalysis.

[7] I. Chorkendorff and J. W. Niemantsverdriet. *Concepts of Modern Catalysis and Kinetics.* Wiley-VCH Verlag GmbH & Co. KGaA, **2005**. doi:10.1002/3527602658.fmatter.

[8] D. King and D. Woodruff, eds. *The chemical physics of solid surfaces and heterogeneous catalysis*, vol. 2. Elsevier, Amsterdam, **1983**.

[9] M. Bowker. *The basis and applications of heterogeneous catalysis.* Oxford University Press, **1998**.

[10] J. A. Dumesic, G. W. Huber, and M. Boudart. *Principles of heterogeneous catalysis.* Handbook of Heterogeneous Catalysis **2008**. doi:10.1002/9783527610044.hetcat0001.

[11] A. T. Bell. *The Impact of Nanoscience on Heterogeneous Catalysis.* Science 299(5613), pp. 1688–1691, **2003**.

[12] C. Giacovazzo, ed. *Fundamentals of Crystallography.* Oxford University Press, **1992**.

[13] J. Gustafson, A. Resta, A. Mikkelsen, R. Westerström, J. N. Andersen, E. Lundgren, J. Weissenrieder, M. Schmid, P. Varga, N. Kasper, X. Torrelles, S. Ferrer, F. Mittendorfer, and G. Kresse. Phys. Rev., B 74, p. 35401, **2006**.

[14] B. Hammer, O. H. Nielsen, and J. Nörskov. Catal. Lett. 46, pp. 31–35, **1997**.

[15] J. Gustafson, M. Borg, A. Mikkelsen, S. Gorovikov, E. Lundgren, and J. N. Andersen. Phys. Rev. Lett. 91, pp. 056102 –, **2003**.

[16] X. F. Ma, H. Su, H. Deng, and W. Li. *Carbon monoxide adsorption and dissociation on Mn-decorated Rh(111) and Rh(553) surfaces: A first-principles study.* Catalysis Today 160, pp. 228–233, **2011**.

[17] J. Y. Park, K. Qadir, and S. M. Kim. *Role of Surface Oxides on Model Nanocatalysts in Catalytic Activity of CO Oxidation*, pp. 145–170. Springer New York, New York, NY, **2014**. doi:10.1007/978-1-4614-8742-5_7.

[18] K. R. Lawless. *The oxidation of metals.* Reports on Progress in Physics 37(2), p. 231, **1974**.

[19] J. F. Weaver. *Surface Chemistry of Late Transition Metal Oxides.* Chemical Reviews 113(6), pp. 4164–4215, **2013**. doi:10.1021/cr300323w.

[20] C. B. Gary Attard. *Surface.* oxford science publications, **1998**.

[21] S. Schwegmann, H. Over, V. De Renzi, and G. Ertl. Surf. Sci. **1997**.

[22] J. Schoiswohl, S. Eck, M. Ramsey, J. N. Andersen, S. Surnev, and F. Netzer. *Vanadium oxide nanostructures on Rh (111): Promotion effect of CO adsorption and oxidation.* Surface science 580(1), pp. 122–136, **2005**.

[23] G. Krenn, I. Bako, and R. Schennach. *CO adsorption and CO and O coadsorption on Rh (111) studied by reflection absorption infrared spectroscopy and density functional theory.* The Journal of chemical physics 124(14), p. 144703, **2006**.

[24] A. Jaworowski, A. Beutler, F. Strisland, R. Nyholm, B. Setlik, D. Heskett, and J. Andersen. *Adsorption sites in O and CO coadsorption phases on Rh (111) investigated by high-resolution core-level photoemission.* Surface science 431(1), pp. 33–41, **1999**.

[25] P. C. Wong, K. C. Hui, M. Y. Zhou, and K. A. R. Mitchell. Surf. Sci. 165, p. L21, **1986**.

[26] K. C. Wong, W. Liu, and K. A. R. Mitchell. Surf. Sci. 360, p. 137, **1996**.

[27] C. H. F. Peden, D. W. Goodman, D. S. Blair, P. J. Berlowitz, G. B. Fisher, and S. H. Oh. J. Phys. Chem. 92, p. 1563, **1988**.

[28] L. Köhler, G. Kresse, M. Schmid, E. Lundgren, J. Gustafson, A. Mikkelsen, M. Borg, J. Yuhara, J. N. Andersen, M. Marsman, and P. Varga. Phys. Rev. Lett. 93, p. 266103, **2004**.

[29] S. K. M. F. S.Eck, C.Castellarin-Cudia. Surf. Sci. 536, pp. 166–167, **2003**.

[30] P. Thiel, E. Williams, J. Yates, and W. Weinberg. *The chemisorption of Co on Rh (111).* Surface Science 84(1), pp. 54–64, **1979**.

[31] R. Schennach, G. Krenn, B. Klötzer, and K. Rendulic. *Adsorption of hydrogen and carbon monoxide on Rh (111)/V surface alloys.* Surface science 540(2), pp. 237–245, **2003**.

[32] A. Beutler, E. Lundgren, R. Nyholm, J. Andersen, B. Setlik, and D. Heskett. *On the adsorption sites for CO on the Rh (111) single crystal surface.* Surface science 371(2-3), pp. 381–389, **1997**.

[33] M. Gierer, A. Barbieri, M. Van Hove, and G. Somorjai. *Structural reanalysis of the Rh (111)+(3× 3) R30-CO and Rh (111)+(2× 2)-3CO phases using automated tensor LEED.* Surface science 391(1-3), pp. 176–182, **1997**.

[34] M. Smedh, A. Beutler, T. Ramsvik, R. Nyholm, M. Borg, J. Andersen, R. Duschek, M. Sock, F. Netzer, and M. Ramsey. *Vibrationally resolved C 1s photoemission from CO absorbed on Rh (111): the investigation of a new chemically shifted C 1s component.* Surface science 491(1), pp. 99–114, **2001**.

[35] A. Beutler, E. Lundgren, R. Nyholm, J. Andersen, B. Setlik, and D. Heskett. *Coverage-and temperature-dependent site occupancy of carbon monoxide on Rh (111) studied by high-resolution core-level photoemission.* Surface science 396(1-3), pp. 117–136, **1998**.

[36] S. Schwegmann, H. Over, V. De Renzi, and G. Ertl. *The atomic geometry of the O and CO+O phases on Rh(111).* Surface Science 375, pp. 91–106, **1996**.

[37] N. Seriani, J. Harl, F. Mittendorfer, and G. Kresse. *A first-principles study of bulk oxide formation on Pd(100).* J. of Chem. Phys. 131(5), p. 054701, **2009**. doi:10.1063/1.3187935.

[38] A. Hellman, A. Resta, N. M. Martin, J. Gustafson, A. Trinchero, P.-A. Carlsson, O. Balmes, R. Felici, R. van Rijn, J. W. M. Frenken, J. N. Andersen, E. Lundgren, and H. Grönbeck. *The Active Phase of Palladium during Methane Oxidation.* J. of Phys. Chem. Lett. 3(6), pp. 678–682, **2012**. doi:10.1021/jz300069s. PMID: 26286272.

[39] J. Rogal, K. Reuter, and M. Scheffler. *Thermodynamic stability of PdO surfaces.* Phys. Rev. B 69, p. 075421, **2004**. doi:10.1103/PhysRevB.69.075421.

[40] J. T. Hirvi, T.-J. J. Kinnunen, M. Suvanto, T. A. Pakkanen, and J. K. Nørskov. *CO oxidation on PdO surfaces.* J. of Phys. Chem. Lett. 133(8), **2010**. doi:10.1063/1.3464481.

[41] E. Lundgren, J. Gustafson, A. Mikkelsen, J. N. Andersen, A. Stierle, H. Dosch, M. Todorova, J. Rogal, K. Reuter, and M. Scheffler. Phys. Rev. Lett. 92, p. 046101, **2004**.

[42] C. Dri, C. Africh, F. Esch, G. Comelli, O. Dubay, L. Köhler, F. Mittendorfer, G. Kresse, P. Dudin, and M. Kiskinova. J. Chem. Phys. 125, p. 94701, **2006**.

[43] S. Blomberg, E. Lundgren, R. Westerström, E. Erdogan, N. Martin, A. Mikkelsen, J. Andersen, F. Mittendorfer, and J. Gustafson. *Structure of the Rh2O3(0001) surface.* Surf. Sci. 606(17), pp. 1416 – 1421, **2012**. doi:https://doi.org/10.1016/j.susc.2012.05.004.

[44] J. Gustafson, R. H. Westerström, O. Balmes, A. Resta, R. van Rijn, X. Torrelles, C. T. Herbschleb, J. Freken, and E. Lundgren. *Catalytic Activity of the Rh Surface Oxide: CO Oxidation over Rh(111) under Realistic Condition.* J.Phys.Chem.C 114, pp. 4580–4583, **2010**.

[45] E. Lundgren, A. Mikkelsen, J. N. Andersen, G. Kresse, M. Schmid, and P. Varga. J. Phys. Cond. Matter 18, p. R481, **2006**.

[46] J. Gustafson, A. Mikkelsen, M. Borg, J. N. Andersen, E. Lundgren, C. Klein, W. Hofer, M. Schmid, P. Varga, L. Köhler, G. Kresse, N. Kasper, A. Stierle, and H. Dosch. Phys. Rev. B 71, p. 115442, **2005**.

[47] J. Gustafson, A. Mikkelsen, M. Borg, E. Lundgren, L. Köhler, G. Kresse, M. Schmid, P. Varga, J. Yuhara, X. Torrelles, C. Quirós, and J. N. Andersen. Phys. Rev. Lett. 92, p. 126102, **2004**.

[48] E. Lundgren, J. Gustafson, A. Resta, J. Weissenrieder, A. Mikkelsen, J. N. Andersen, L. Köhler, G. Kresse, J. Klikovits, A. Biederman, M. Schmid, and P. Varga. J. Electron Spectrosc. Relat. Phenom. 144-147, p. 367, **2005**.

[49] C. Africh, F. Esch, W. X. Li, M. Corso, B. Hammer, R. Rosei, and G. Comelli. *Two-Step Reaction on a Strained, Nanoscale Segmented Surface*. Phys. Rev. Lett. 93, p. 126104, **2004**. doi:10.1103/PhysRevLett.93.126104.

[50] C. Africh, L. Köhler, F. Esch, M. Corso, C. Dri, T. Bucko, G. Kresse, and G. Comelli. *Effects of Lattice Expansion on the Reactivity of a One-Dimensional Oxide*. J. Amer. Chem. Soc. 131(9), pp. 3253–3259, **2009**. doi:10.1021/ja808100f. PMID: 19173644.

[51] G. Comelli, V. Dhanak, M. Kiskinova, K. Prince, and R. Rosei. *Oxygen and nitrogen interaction with rhodium single crystal surfaces*. Sur. Sci. Rep. 32, pp. 165 – 231, **1998**. doi:0.1016/S0167-5729(98)00003-X.

[52] E. Vesselli, C. Africh, A. Baraldi, G. Comelli, F. Esch, and R. Rosei. *(102) strained reconstruction induced by oxygen adsorption on the Rh(110) surface*. J. Chem. Phys. 114(9), pp. 4221–4225, **2001**. doi:10.1063/1.1345909.

[53] J. Gustafson, A. Resta, A. Mikkelsen, R. Westerström, J. N. Andersen, E. Lundgren, J. Weissenrieder, M. Schmid, P. Varga, N. Kasper, *et al. Oxygen-induced step bunching and faceting of Rh (553): Experiment and ab initio calculations*. Physical Review B 74(3), p. 035401, **2006**.

[54] J. Klikovits, M. Schmid, L. R. Merte, P. Varga, R. Westerström, A. Resta, J. N. Andersen, J. Gustafson, A. Mikkelsen, E. Lundgren, F. Mittendorfer, and G. Kresse. Phys. Rev. Lett. 101, p. 266104, **2008**.

[55] G. A. Somorjai and Y. M. Li. *Introduction to Surface Chemistry and Catalysis*. Wiley, New York, **2010**.

[56] F. Mittendorfer. J. Phys.: Condens. Matter 22, p. 393001, **2010**.

[57] N. Martin. *Surface Studies of Model Systems Relevant for Pd and Ag Catalysts*. Ph.D. thesis, Lund University, **2014**.

[58] J. Gustafson, R. Westerström, O. Balmes, A. Resta, R. van Rijn, X. Torrelles, C. T. Herbschleb, J. W. M. Frenken, and E. Lundgren. J. Phys. Chem. C 114, p. 4580, **2010**.

[59] C. J. Laidler and J. H. Meiser. *Physical Chemistry*. **1982**.

[60] I. Langmuir. *The mechanism of the catalytic action of platinum in the reactions* $2CO + O_2 = 2CO_2$ *and* $2H_2 + O_2 = 2H_2O$. Transactions of the Faraday Society 17, pp. 621–654, **1922**.

[61] I. K. Robinson, R. T. Tung, and R. Feidenhans'l. *X-ray interference method for studying interface structures*. Phys. Rev. B: Condens. Matter 38, pp. 3632–3635, **1988**. doi:10.1103/PhysRevB.38.3632.

[62] L. C. Feldman and J. W. Mayer. *Fundamentals of Surface Thin Film Analysis*. Pearson Education (US), **1986**.

[63] H. Bubert, J. C. Riviére, H. F. Arlinghaus, H. Hutter, H. Jenett, P. Bauer, L. Palmetshofer, L. Fabry, S. Pahlke, A. Quentmeier, K. Hinrichs, W. Hill, B. Gruska, A. Röseler, and G. Friedbacher. *Surface and Thin Film Analysis*. Wiley-VCH, Weinheim - Germany, **2000**. doi:10.1002/14356007.b06_023.

[64] J. S. H. Hideo. Iwai and T. Shigeo. J. Surf. Anal. 15, pp. 264–270, **2009**.

[65] A. Thompson, ed. *X-ray Data Booklet*. Lawrence Berkeley National Laboratory, University of California, Berkeley, CA, USA, **2009**.

[66] C. Wagner, W. Riggs, L. Davis, J. Moulder, and G. Muilenberg. *Handbook of X-ray Photoelectron Spectroscopy*. Perkin-Elmer Corporation: Eden Prairie, MN, USA, **1979**.

[67] E. Vlieg, J. V. D. Veen, S. Gurman, C. Norris, and J. Macdonald. *X-ray diffraction from rough, relaxed and reconstructed surfaces*. Surf. Sci. 210(3), pp. 301 – 321, **1989**. doi:10.1016/0039-6028(89)90598-0.

[68] R. Feidenhans'l. *Surface structure determination by X-ray diffraction*. Surf. Sci. Rep. 10(3), pp. 105 – 188, **1989**. doi:10.1016/0167-5729(89)90002-2.

[69] V. K. Pecharsky and P. Zavalij. *Properties, Sources, and Detection of Radiation*. oxford science publications, **2008**.

[70] D. J. T. K. Robinson. *Surface X-ray diffraction*. Rep Prog Phys 55, pp. 599–651, **1992**.

[71] J. Atkins Peter, de Paula. *Atkins' Physical Chemistry, 10th edition.* Oxford University Press, Oxford, **2014**.

[72] http://pd.chem.ucl.ac.uk/pdnn/diff1/scate2.htm. *School of Crystallography, Birkbeck College, University of London.*

[73] W. H. Bragg and W. L. Bragg. *The Reflection of X-rays by Crystals.* Proc. R. Soc. Lond. A 88(605), pp. 428–438, **1913**. doi:10.1098/rspa.1913.0040.

[74] C. M. Schlepütz, S. O. Mariager, S. A. Pauli, R. Feidenhans'l, and P. R. Willmott. *Angle calculations for a (2+3)-type diffractometer: focus on area detectors.* J. Appl. Crystallogr. 44, pp. 73–83, **2011**. doi:10.1107/S0021889810048922.

[75] S. Tanuma, C. J. Powell, and D. R. Penn. *Calculations of electron inelastic mean free paths (IMFPS). IV. Evaluation of calculated IMFPs and of the predictive IMFP formula TPP-2 for electron energies between 50 and 2000 eV.* Surf. Interface Anal. 20(1), pp. 77–89, **1993**. doi:10.1002/sia.740200112.

[76] M. P. Seah and W. A. Dench. *Quantitative electron spectroscopy of surfaces: A standard data base for electron inelastic mean free paths in solids.* Surf. Interface Anal. 1(1), pp. 2–11, **1979**. doi:10.1002/sia.740010103.

[77] C. D. Wagner, L. E. Davis, and W. M. Riggs. *The energy dependence of the electron mean free path.* Surface and Interface Analysis 2(2), pp. 53–55, **1980**. doi:10.1002/sia.740020204.

[78] F. Jona. *LEED Crystallography.* J. Phys. C: Solid State Phys. 11(21), pp. 4271–4306, **1978**.

[79] H. Lüth. *Surface and Interfaces of Solid Materials.* Springer-Verlag Berlin Heidelberg New York, **1995**.

[80] I. K. Robinson. Phys. Rev. B 33, p. 3830, **1986**.

[81] I. Chorkendorff and J. W. Niemantsverdriet. *Concepts of Modern Catalysis and Kinetics.* Wiley-VCH Verlag GmbH & Co. KGaA, **2007**.

[82] E. Willett. *The Basics of Quantum Physics: Understanding the Photoelectric Effect and Line Spectra.* The Rosen Publishing Group, **2004**.

[83] K. Siegbahn. *Electron Spectroscopy for atoms, molecules and condensed matter.* Nobel lecture **1981**.

[84] S. Doniach and M. Sunjic. *Many-electron singularity in X-ray photoemission and X-ray line spectra from metals.* J. Phys. C: Solid State Phys. 3(2), p. 285, **1970**.

[85] S. Hofmann. Springer Science Business Medi **2012**.

[86] www.sljus.lu.se. *FitXPS software.*

[87] N. W. Ashcroft and N. D. Mermin. *Solid state physics.* Holt, Rinehart and Winston, Philadelphia, USA, **1976**.

[88] https://en.wikipedia.org. *Franck–Condon principle.*

[89] S. Blomberg, J. Zetterberg, J. Zhou, L. R. Merte, J. Gustafson, M. Shipilin, A. Trinchero, L. Miccio, A. Magaña, M. Ilyn, *et al. Strain dependent light-off temperature in catalysis revealed by planar laser-induced fluorescence.* ACS Catalysis 7(1), pp. 110–114, **2016**.

[90] H. V. Dam, L. Wisse, and H. V. Bekkum. *Platinum/carbon oxidation catalysts: VIII. Selecting a metal for liquid-phase alcohol oxidations.* Appl. Catal. 61(1), pp. 187 – 197, **1990**. doi:https://doi.org/10.1016/S0166-9834(00)82143-0.